5 Using CFD to Investigate Remedial Measures for Boiler Tube Erosion

5.1 Introduction

All the research done so far in this thesis supports the research to be presented in this chapter, and served to give a broad background on erosion in boilers. In Chapter 3, the mechanisms of boiler tube failures were discussed. As erosion is identified as the leading cause of boiler tube failures at Sasol, the mechanisms of erosion were investigated in detail. Remedial measures proposed by other researchers were then investigated. In Chapter 4, two-phase flow was investigated in tube banks. Numerical simulations of other researchers were studied to see which size particles contribute the most to tube erosion. Boiler CFD modelling done by other researchers were then discussed. A CFD parametric study was done to see what influence certain operating conditions had on boiler flows. It was clear that larger particles were flung outwards towards the top of the boiler and are probably the cause of erosion in those areas. In this chapter ways are investigated from the knowledge gained so far in this study to solve the unique erosion problems encountered in the boilers at Sasol.

5.2 Erosion in Centre of the Tube Bank

5.2.1 Introduction

A useful first analysis is to recreate the flow conditions in the tube bank without any remedial measures. If the location of erosion can be predicted in this CFD analysis and it relates to observed erosion patterns during boiler shutdown, then remedial measures can be implemented in the CFD boiler model to minimise erosion.

5.2.2 Flow in the Center of Tube Bank without Remedial Measures

Figure 5-1 illustrates the horizontal cross section of the boiler bank at the centre of the boiler. There is a larger than usual gap in the centre of the boiler. There is also a large gap between the tube banks in the horizontal plane. This gap is aligned 90° to the flow direction. The computational domain for the CFD model is the green crosshatched region in Figure 5-1 with symmetrical boundaries to the left and right of the domain. The 8 tube rows on the right of the computational domain have a coarser grid due to memory limitations, while a fine grid is used for the 6 tube rows next to the centre gap. The computational domain illustrated in Figure 5-1 consists of 374812 cells. Incompressible air is used as the fluid in this study. The computational grid around one tube of the denser grid is illustrated Figure 5-2.

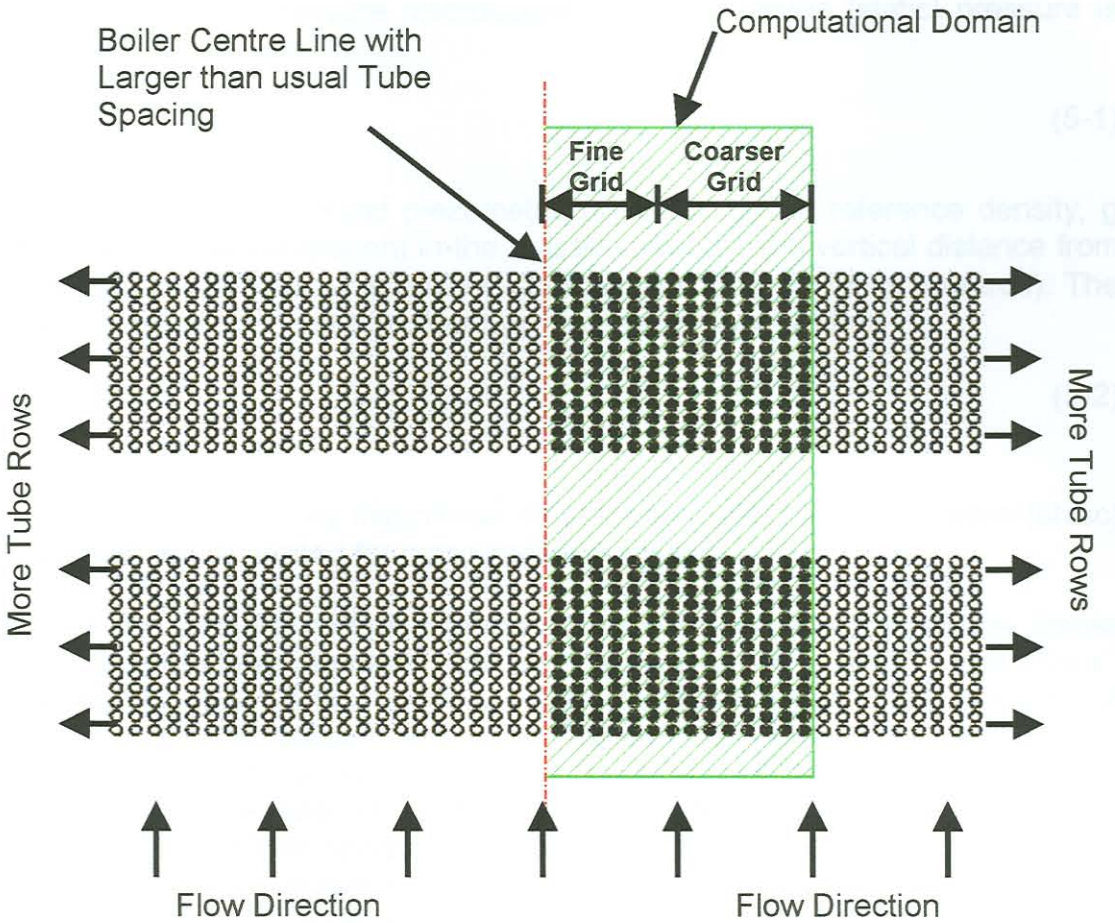

Figure 5-1 Computational Domain of Centre of Boiler Bank

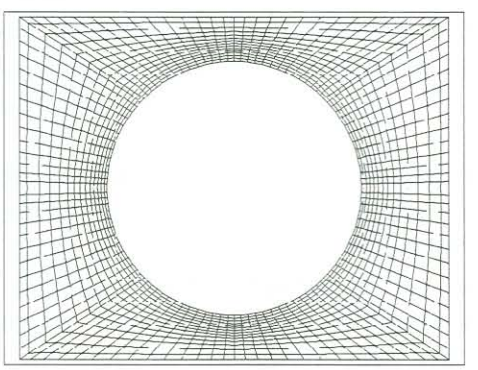

Figure 5-2 Computational Grid around One Tube in the Boiler Bank (Fine Grid)

The pressure distribution across the computational domain is a good indication that the interface between grids with different densities is of an appropriate quality. If sudden changes do not occur in the pressure distribution across grid interfaces of different densities then the grid interface is usually of an appropriate quality.

The four following pictures indicate the piezometric pressure distribution and the total relative pressure distributions. The piezometric (static) pressure is calcutated as follows:

$$p_s = p_p + \rho_0 g z \tag{5-1}$$

where p_p is the computed piezometric pressure, ρ_0 the reference density, g the gravitational component in the z-direction and z the vertical distance from a datum level where ρ_0 is defined (the z-axis points vertically upwards). The total pressure for incompressible flow is calculated as follows:

$$p_{tot} = p_s + \frac{1}{2}\rho V^2 \tag{5-2}$$

where V is the velocity magnitude. Both these pressures, piezometric (static) and total, are illustrated for comparative purposes.

Figure 5-3 and Figure 5-4 give the piezometric pressure distribution across the computational domain for inlet velocities of $10m.s^{-1}$ and $5m.s^{-1}$ respectively. The vertical black line indicates the position where the grids of different densities meet. There is no indication of sudden pressure changes across the interface indicated by the black line of different grid densities. Figure 5-5 and Figure 5-6 illustrate the total relative pressure distribution for the two different inlet conditions. Once again, there is no indication of sudden pressure changes across the interface. It can therefore be assumed that the interface between the different cell densities at the interface is appropriate.

The velocity magnitude distribution can be seen in Figure 5-7 and Figure 5-8 for different inlet velocities of $10m.s^{-1}$ and $5m.s^{-1}$ respectively. It can be seen from these figures that there are high peak velocities in the centre gap of the tube bank for both cases. It is also evident that the higher velocity magnitude region extends a few tube rows adjacent to both the centre gap as well as the gap between the two tube bundles.

The velocity magnitude at the right of the computational domain for both cases is very low. The blue regions on the velocity magnitude plots indicate this low velocity. This is due to the chosen boundary conditions. The best possible solution would have been obtained if the whole boiler bank were included in the CFD model. Due to memory limitations this was not possible. Because the velocities are high in the centre gap the mass flow is greater in this region. As a consequence, for the continuity equations to be satisfied, the flow rate must be less at the boundary furthest away from the centre gap. As the region of interest is close to the centre gap, the boundary conditions assumption is sufficient to provide quantitative results. Other boundary conditions or larger tube banks with coarser grids can be investigated in the future.

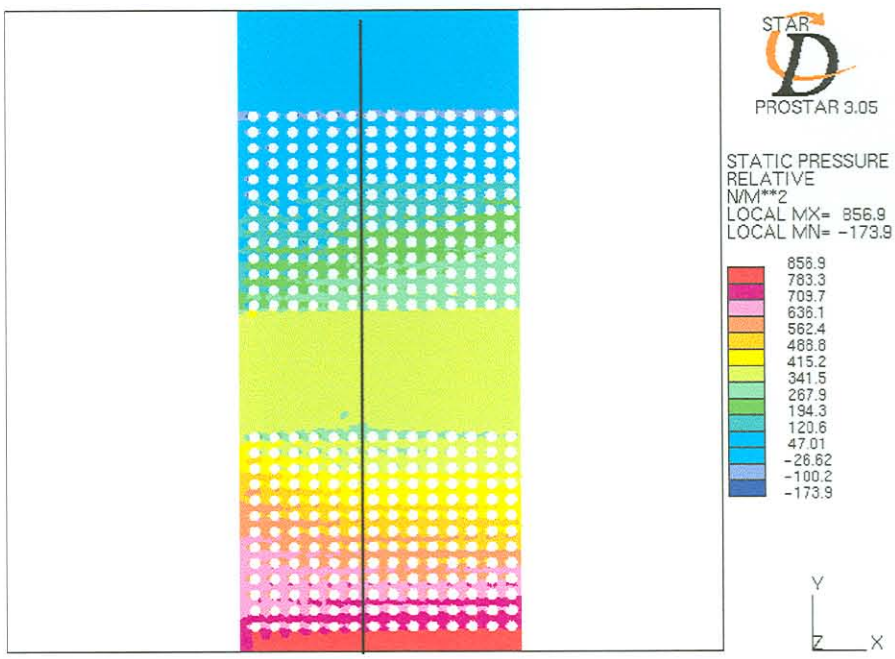

Figure 5-3 Piezometric Pressure Distribution for Flow across the Whole Computational Domain for 10m.s^{-1} Inlet Velocity

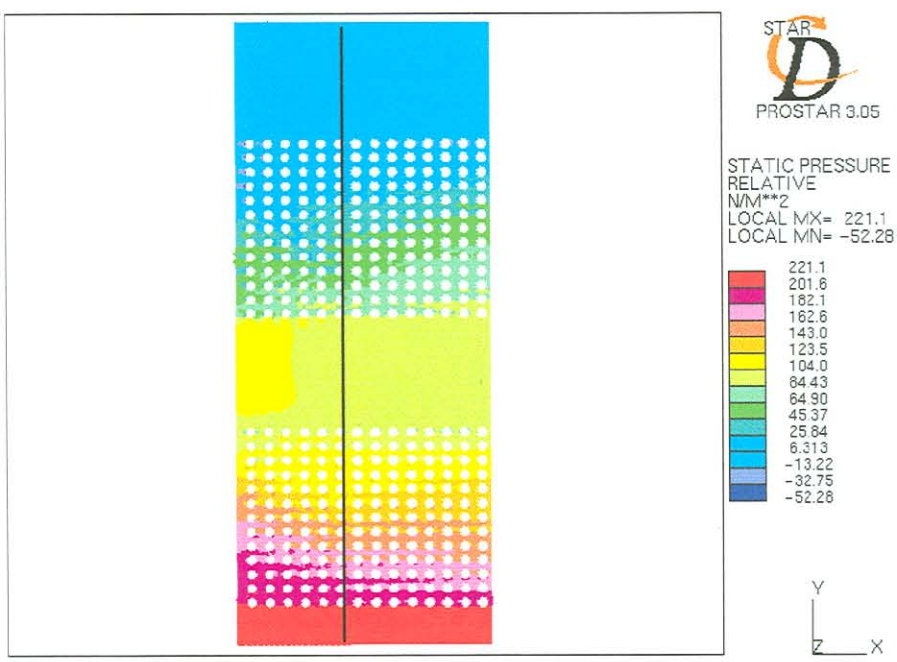

Figure 5-4 Piezometric Pressure Distribution for Flow across the Whole Computational Domain for 5m.s^{-1} Inlet Velocity

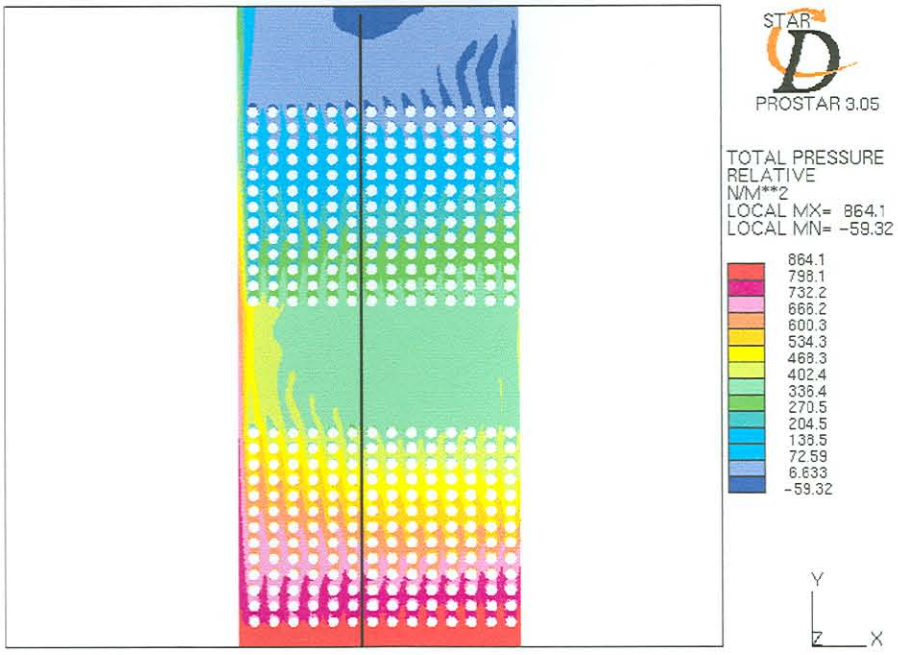

Figure 5-5 Total Relative Pressure Distribution for Flow across the Whole Computational Domain for 10m.s^{-1} Inlet Velocity

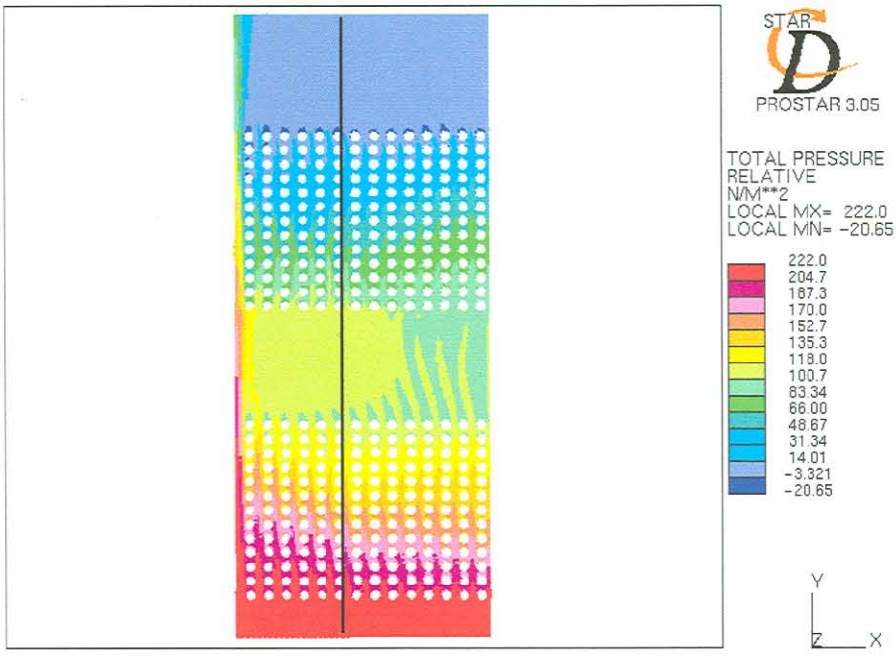

Figure 5-6 Total Relative Pressure Distribution for Flow across the Whole Computational Domain for 5m.s^{-1} Inlet Velocity

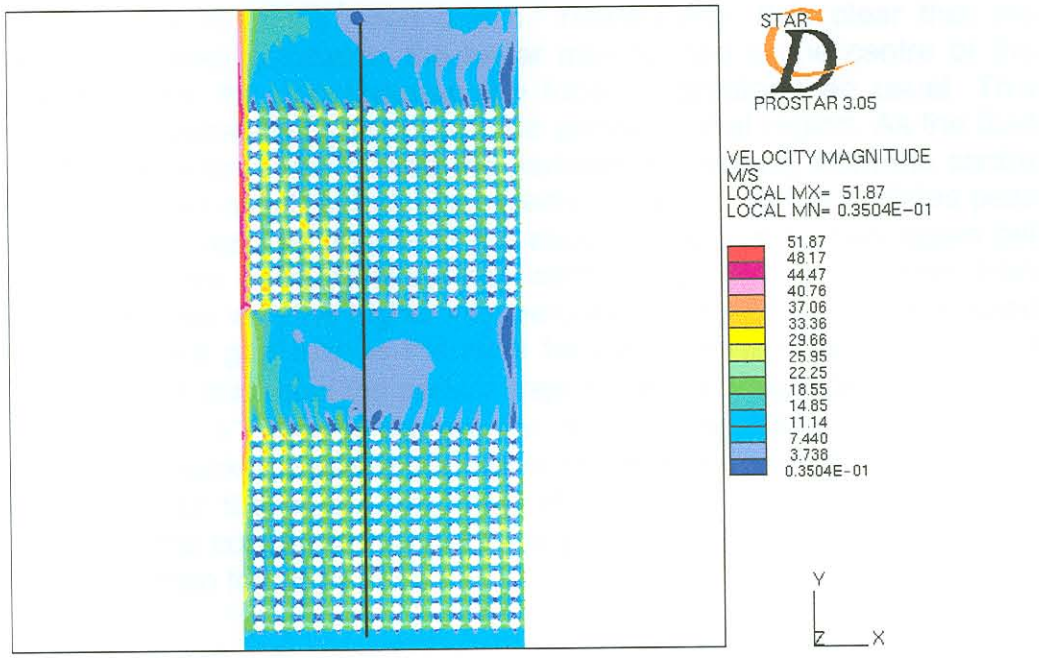

Figure 5-7 Velocity Magnitude Contour Plot for Flow across the Whole Computational Domain for 10m.s^{-1} Inlet Velocity

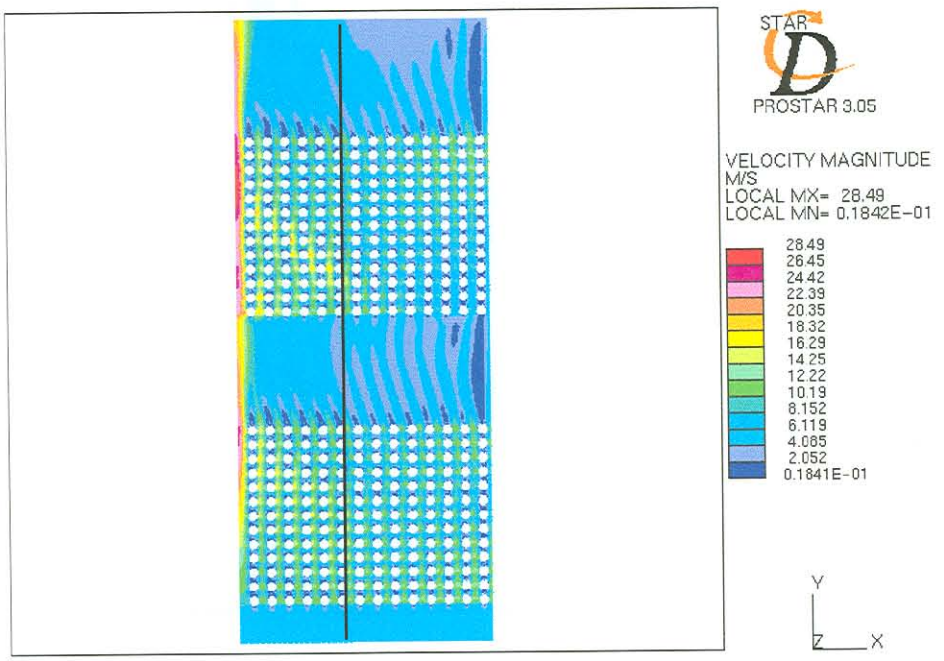

Figure 5-8 Velocity Magnitude Contour Plot for Flow across the Whole Computational Domain for 5m.s^{-1} Inlet Velocity

Figure 5-9 and Figure 5-10 illustrate the particle trajectories for 10μm particles at inlet velocities of 10m.s^{-1} and 5 m.s^{-1} respectively. It is clear that the particles are sucked in towards the faster moving fluid in the centre of the boiler bank where the gap between the tubes is greater than usual. This causes the concentration of particles to be greater in that region. As the fluid moves into the second tube bundle the particles move away from the centre gap and tend to get redistributed more evenly. However, as the particles pass approximately through the middle of the second tube bundle they again get sucked to the centre because of the high centre velocity. It can be seen from Figure 5-9, the case with the higher inlet velocity, that the particles get sucked more to the centre gap than is the case for the lower inlet velocity (Figure 5-10). Figure 5-11 illustrates the particle trajectories for 100μm particles with a inlet velocity of 5m.s^{-1}. Due to the greater inertia of the 100μm particles, the particles are not sucked towards the centre of the boiler bank as much as the 10μm particles for the same conditions (Figure 5-10). It can therefore be concluded that the concentration of smaller particles is higher in the centre of the boiler bank than for larger particles.

These results prove that the CFD solution predicts erosion in the region of observed erosion patterns during boiler shutdown. This is the case, because, as already discussed, erosion is a linear function of particle concentration and a function of velocity to the power of two to four. As the velocity and particle concentration is high in the centre of the boiler, erosion will be more prevalent in this region.

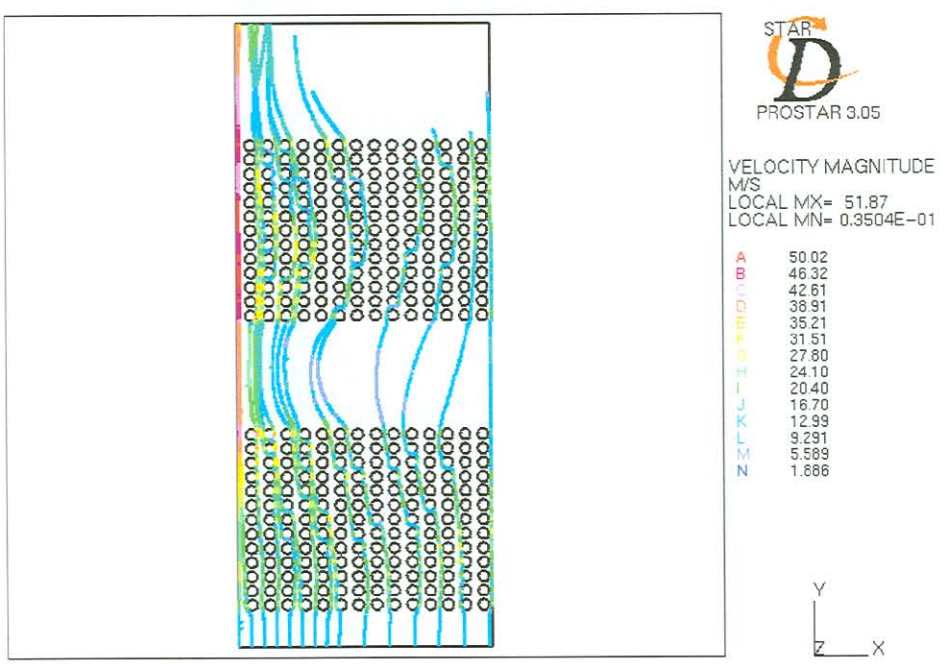

Figure 5-9 Particle Trajectories for 10μm Particles for 10m.s^{-1} Inlet Velocity

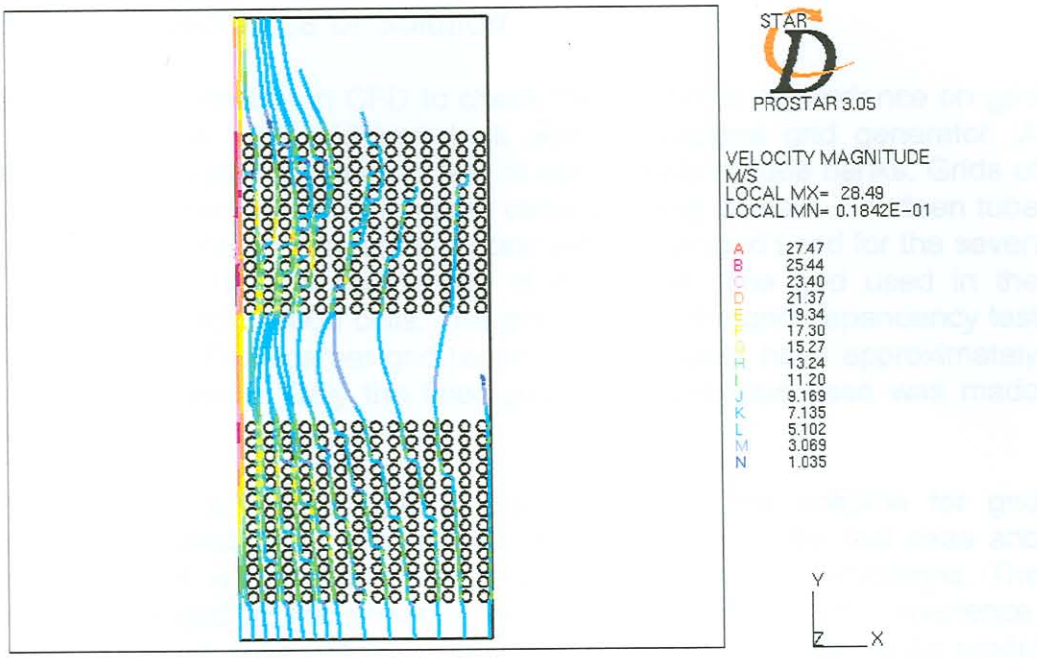

Figure 5-10 Particle Trajectories for 10μm Particles for 5m.s^{-1} Inlet Velocity

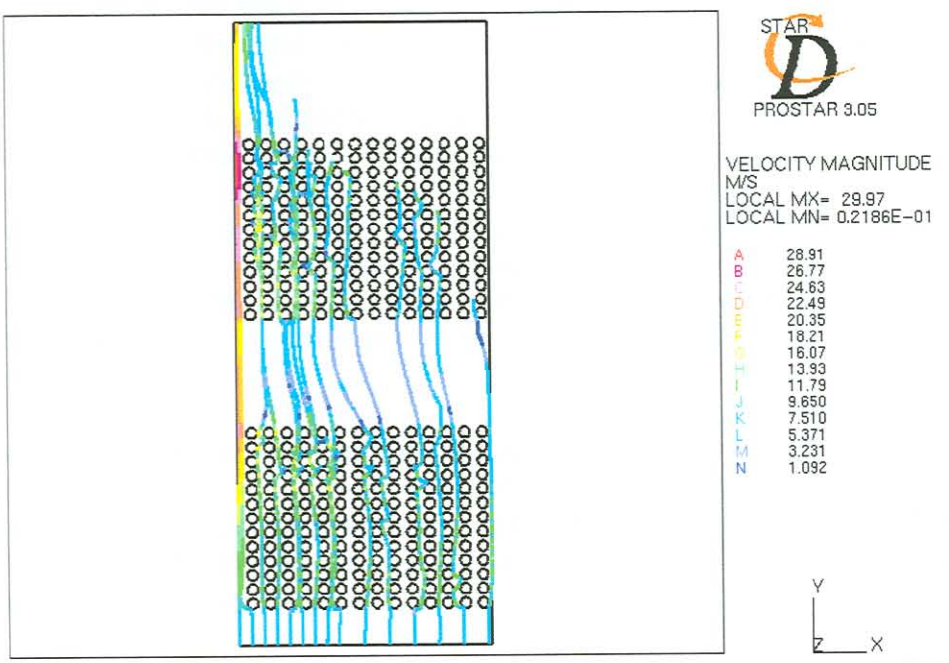

Figure 5-11 Particle Trajectories for 100μm Particles for 5m.s^{-1} Inlet Velocity

5.2.3 Grid Dependence of Solution

It is always good practice in CFD to check the solution's dependence on grid size and shape. A new grid was built with an elliptical grid generator. A elliptical grid generator are used to test its applicability to tube banks. Grids of two sizes were again used in the same computational domain. Fourteen tube rows are used for the grid dependency test with a finer grid used for the seven tube rows nearest to the centre gap of the boiler. The grid used in the previous section had 375000 cells. The grid used for the grid dependency test has 243000 cells. The coarser grid regions of both grids have approximately the same grid density. Only the finer grid of the previous case was made coarser.

The reason why a coarser grid is used to check the solution for grid dependence is because a relatively fine grid was used in the first case and further refinement is not possible due to computer memory limitations. The fineness of the grid in the previous section was chosen from experience. When the pressure drop characteristics was obtained in the hydraulic model of the tube bank to obtain porosity coefficients, it was concluded that a fine grid was necessary to obtain the correct separation point on each tube.

Figure 5-12 and Figure 5-13 show the piezometric and total pressure distributions respectively. If these results are compared to Figure 5-3 and Figure 5-5 it can be seen that the pressure distributions are very similar. The pressure drop across the tube bank for this grid is approximately 2% less than was the case for the grid used in Chapter 5.2.1. As a difference of 2% is acceptable for the purposes of this study it can be concluded that the finer grid used in the previous section is appropriate for this study and that further grid refinement to the fine grid will not increase solution accuracy significantly.

Figure 5-14 shows the velocity magnitude plot for the coarser elliptical grid used. If this figure is compared to Figure 5-7 it can be seen that there is an approximately 6% difference in the maximum velocity obtained where the maximum velocity of the finer grid is higher than the maximum velocity of the coarser grid.

Figure 5-15 illustrates the particle trajectories of 10μm particles for the case where a coarser grid was used. If this solution is compared to Figure 5-9 that shows the solution for the same case but with a finer grid it can be seen that the particles are sucked in more towards the centre of the boiler bank as was the case with the coarser grid.

It can be concluded that the finer grid is acceptable for accurate CFD results. The fine grid has 54% more cells than the coarser grid but the maximum pressures for the two cases differ by only 2% and the maximum velocities differ by only 6%. As grid refinement to the finer grid will increase solution time significantly, the results will not change much though. The fine grid used in Chapter 5.2.1 is thus acceptable and further grid refinement to the fine grid will not greatly influence the solution.

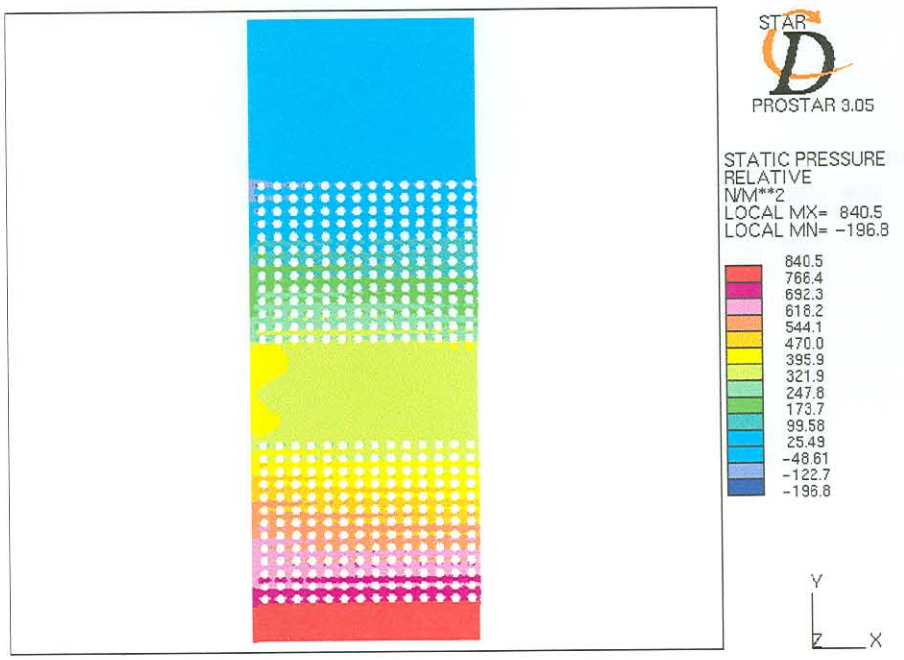

Figure 5-12 Piezometric Pressure Contours for Elliptical Grid for a 10ms^{-1} Inlet Velocity – Coarser Grid

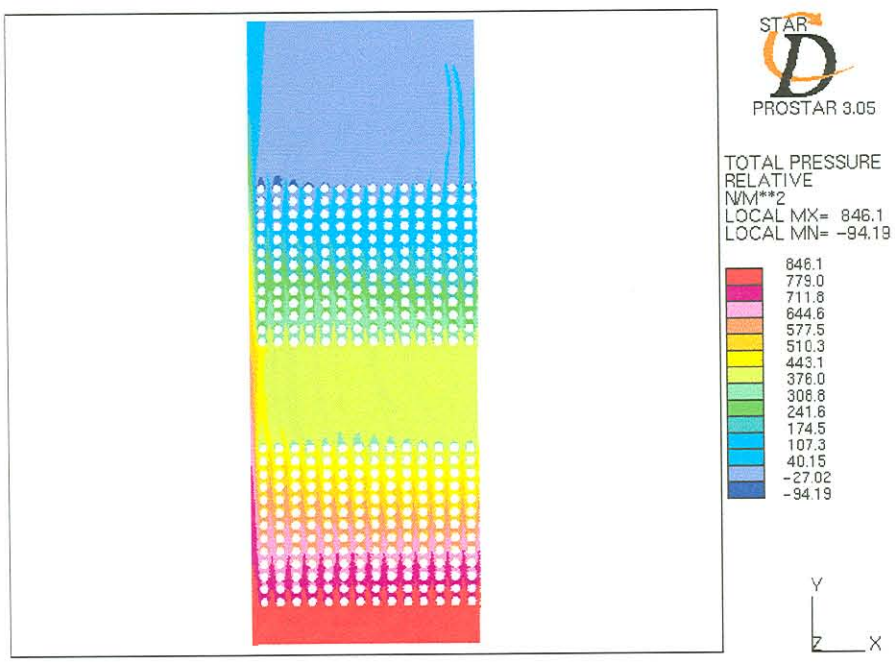

Figure 5-13 Total Pressure Contours for Elliptical Grid for a 10ms^{-1} Inlet Velocity – Coarser Grid

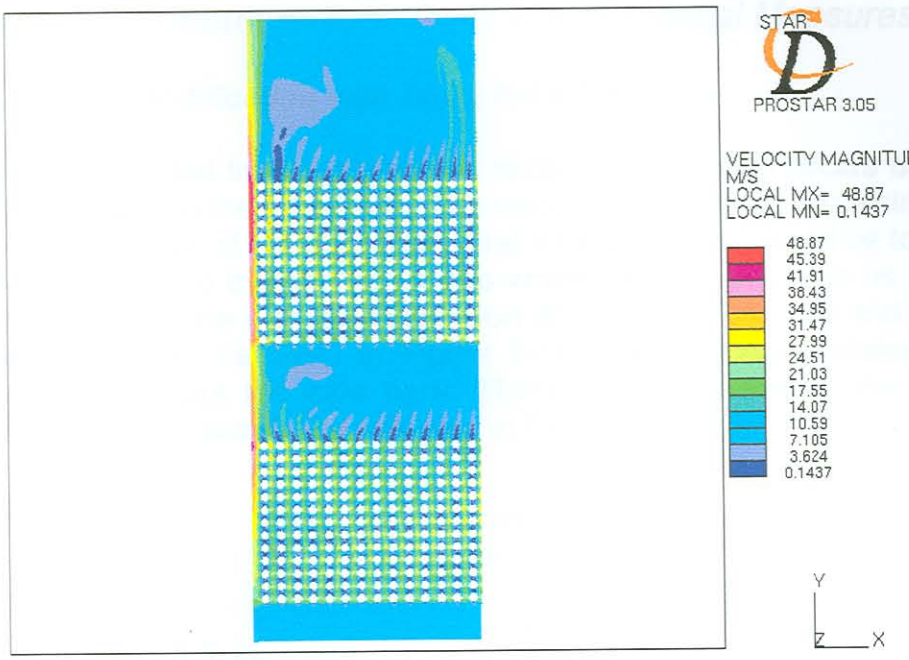

Figure 5-14 Velocity Magnitude Contours for Elliptical Grid for a 10ms^{-1} Inlet Velocity – Coarser Grid

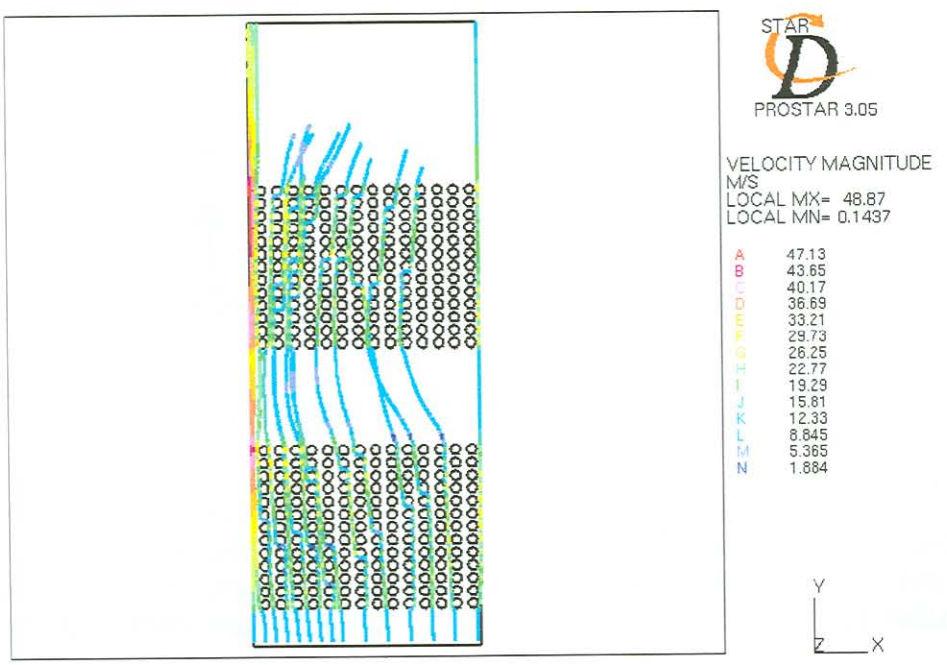

Figure 5-15 Partical Traces for 10μm Particles with a 10ms^{-1} Inlet Velocity - Coarser Grid

5.2.4 Flow in Centre of Tube Bank with Remedial Measures

5.2.4.1 Flow-Modification with Eight Tube Fins

It can be concluded from the previous section that erosion occurs due to the effect of the gap in the tube bank. The velocity and particle concentration are higher in the region of the gap. One's first intuitive feeling would be to suggest to cover the gap so that the larger gap would be the same size as the other gaps. This was done with the installation of tube fins. The size and shape of the fins used can be seen in Figure 5-16. The fins are installed at four locations throughout the tube bank. The fins are installed at the inlet and outlet of each tube bundle as indicated in Figure 5-17.

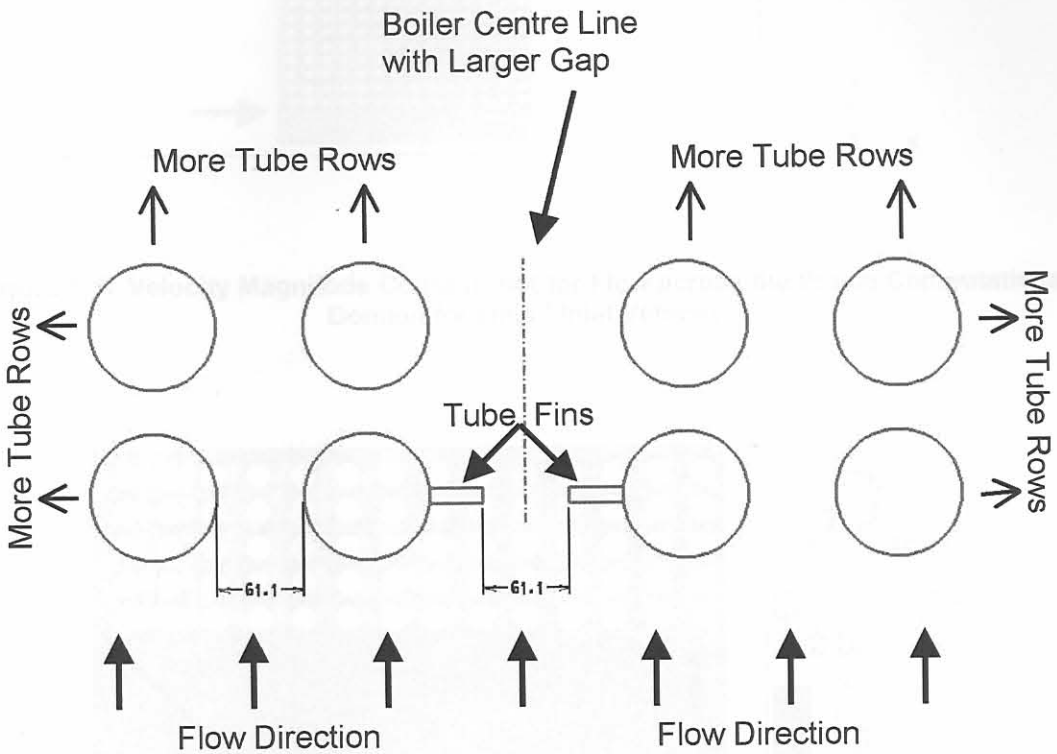

Figure 5-16 Position of Tube Fins

Figure 5-17 illustrates the velocity magnitude plot across the whole computational domain for an inlet velocity of 5m.s^{-1}. The maximum velocity in the domain is 24.13m.s^{-1}. The maximum velocity obtained in the case where no fins were used was 28.49m.s^{-1}. The maximum velocity is thus reduced by 15.3%.

Figure 5-18 is a close-up view of the flow in the centre of the tube bank. It can be seen that the fin at the outlet of the first tube bundle deflects the flow onto adjacent tubes, which can lead to degradation of those tubes. The same is happening at the outlet of the second tube bundle as shown in Figure 5-19.

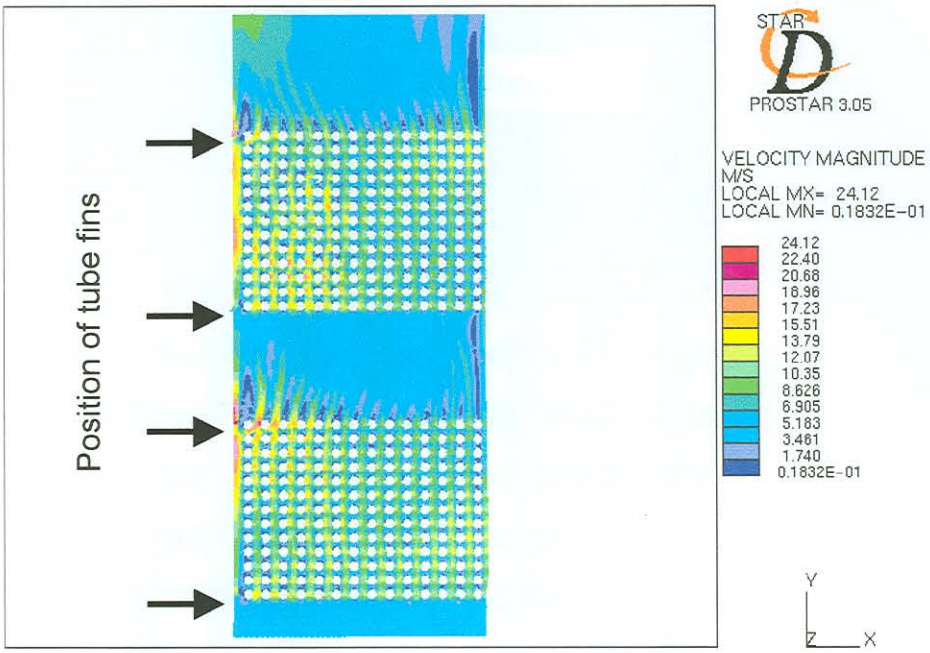

Figure 5-17 Velocity Magnitude Contour Plot for Flow across the Whole Computational Domain for 5m.s^{-1} Inlet Velocity

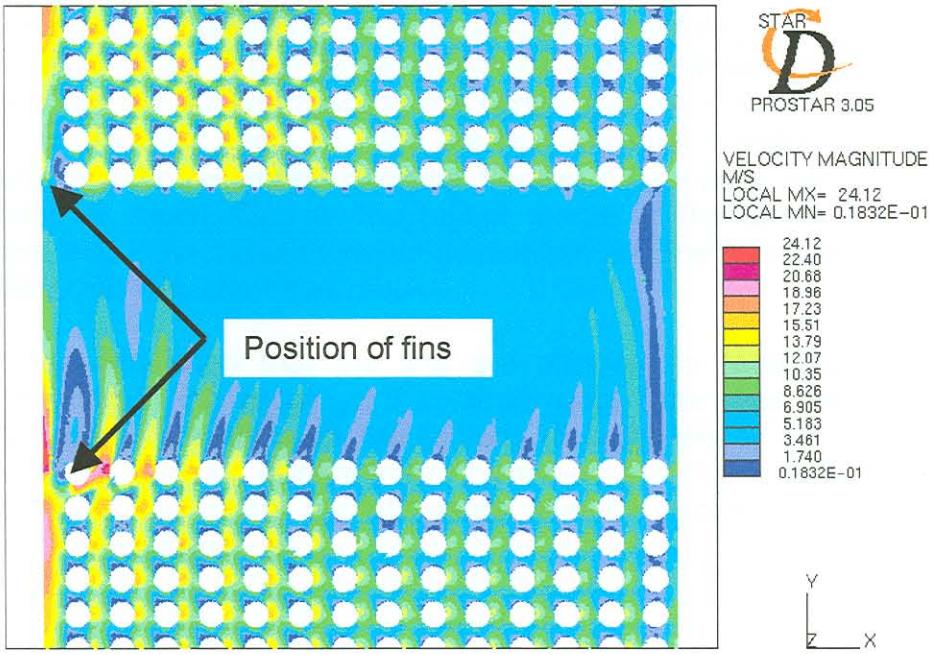

Figure 5-18 Velocity Magnitude Contour Plot for Flow in the Centre of the Tube Bank

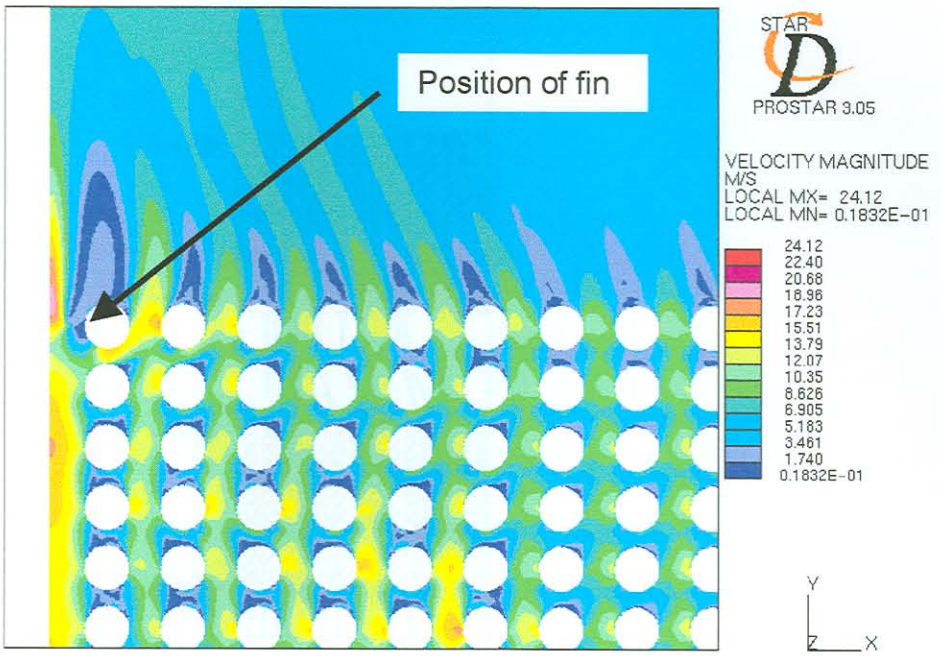

Figure 5-19 Velocity Magnitude Contour Plot for Flow at the Outlet of the Tube Bank

Figure 5-20 and Figure 5-21 show the particle traces for 100μm and 10μm particles respectively for the case where eight fins are used in the CFD model. If these results are compared to Figure 5-10 and Figure 5-11, which are the particle traces of 10μm and 100μm particles respectively for the case where no fins were used, it can be seen that the particle traces differ. The 10μm particles are not sucked towards the centre gap as much as was the case where no fins were used. The fins are thus effective in reducing the particle concentration for the smaller particles. For the 100μm particles, the results do not differ as much. Due to the higher inertia of the larger particles, the particles tend to keep their forward momentum and the effect of the gap does not effect their trajectories as much.

It can be concluded that the fins are effective in reducing the particle concentration in the region of the centre gap. Care must be taken when installing these fins because the regions of high velocity can be shifted to adjacent tubes as was evident from Figure 5-18 and Figure 5-19. Channelling of the flow in the centre gap still exists after the modelling of eight fins to prevent this problem.

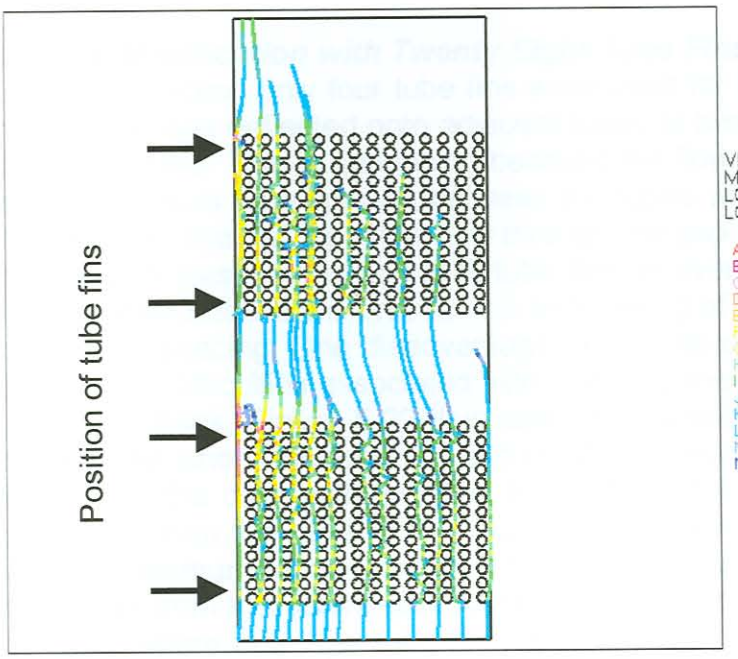

Figure 5-20 Particle Trajectories for 100μm Particles for 5m.s^{-1} Inlet Velocity

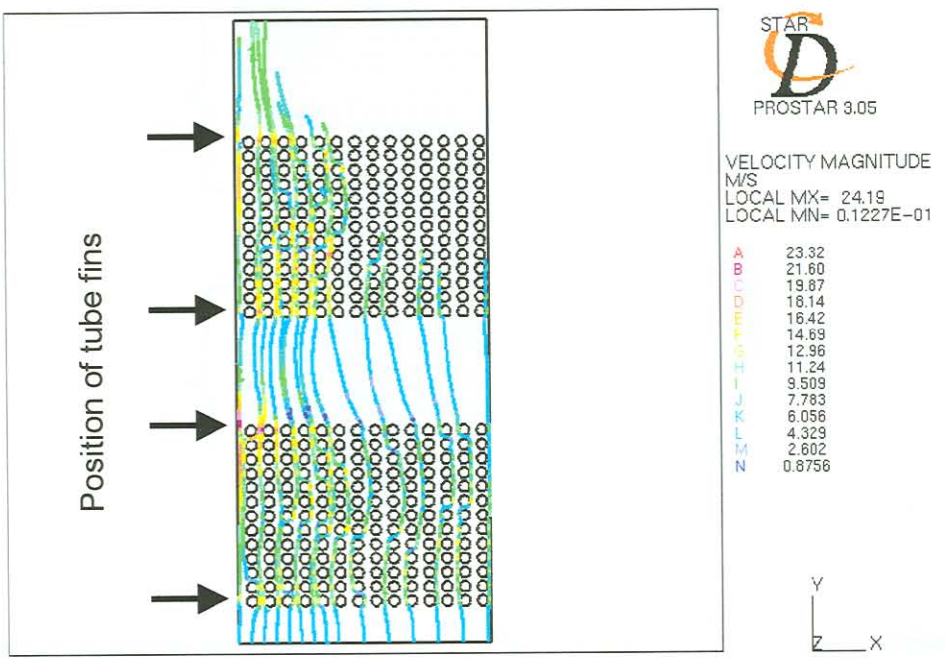

Figure 5-21 Particle Trajectories for 10μm Particles for 5m.s^{-1} Inlet Velocity

5.2.4.2 Flow-Modification with Twenty Eight Tube Fins

In the previous section only four tube fins were used for the symmetrical half shown. The flow was deflected onto adjacent tubes at two locations at the exit of each tube bundle. This is happening because the flow is still channelling in the larger than usual tube spacing between the tubes with the fins. One way of eliminating the channelling of the flow through the gap is through the use of more tube fins. It was decided to install tube fins on every second tube in the gap with the idea that this will prevent the channelling of the flow in the larger than usual tube spacing. One disadvantage of the use of fins throughout the tube bank is the difficulties associated with installing the tubes with fins deep within the tube bank. Figure 5-22 illustrates the velocity magnitude contour plot for the case where fourteen fins are used. The maximum velocity in the flow domain for the case with fourteen fins is 23.59m.s^{-1}. This represents a 2.2% decrease from the case where four tube fins were used, and a 17.2% decrease in maximum velocity where no fins were used. Again the flow is deflected away from the centre gap by the tube fins but to a lesser extent as was the case where only four tube fins were used. This can be seen in the close-up view in Figure 5-23.

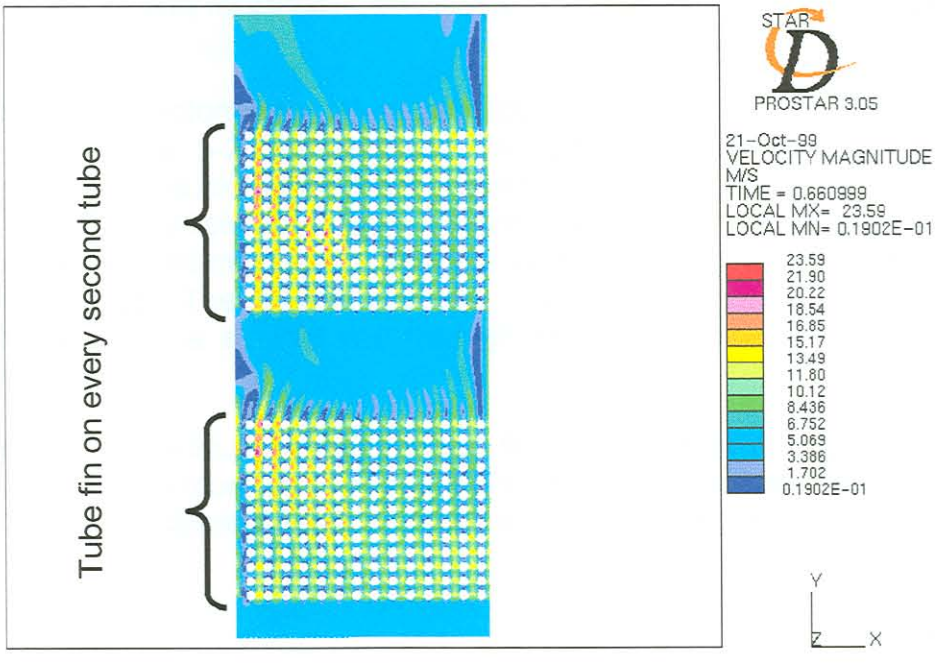

Figure 5-22 Velocity Magnitude Contour Plot for Flow across the Whole Computational Domain for 5m.s^{-1} Inlet Velocity

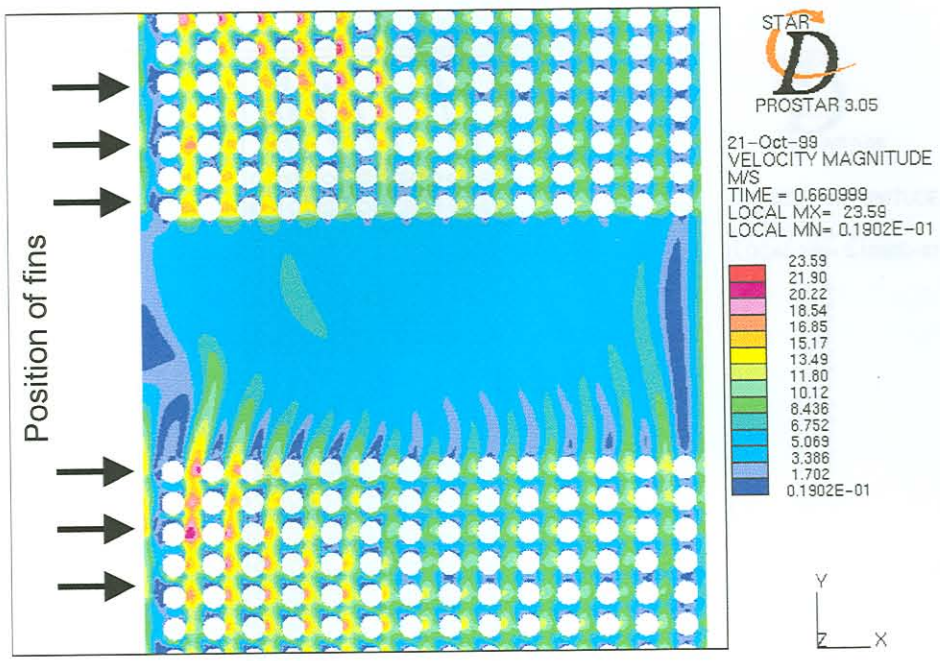

Figure 5-23 Velocity Magnitude Contour Plot for Flow in the Centre of the Tube Bank

The particle trajectories for 10μm and 100μm particles can be seen in Figure 5-24 and Figure 5-25 respectively. The particle trajectories of the 10μm particles are not sucked towards the centre gap as was the case with the four tube fins. The particle trajectories behave somewhat strange due to the fact that some particles move away from the centre gap and others move towards the centre gap. The 100μm particles, as with the previous cases, move approximately in a straight line through the tube bank due to their higher inertia.

This remedial measure where 14 tube fins are used, is a very viable option because the maximum velocity in the flow domain is reduced. The flow is not deflected onto adjacent tubes as much as the case where four tube fins were used.

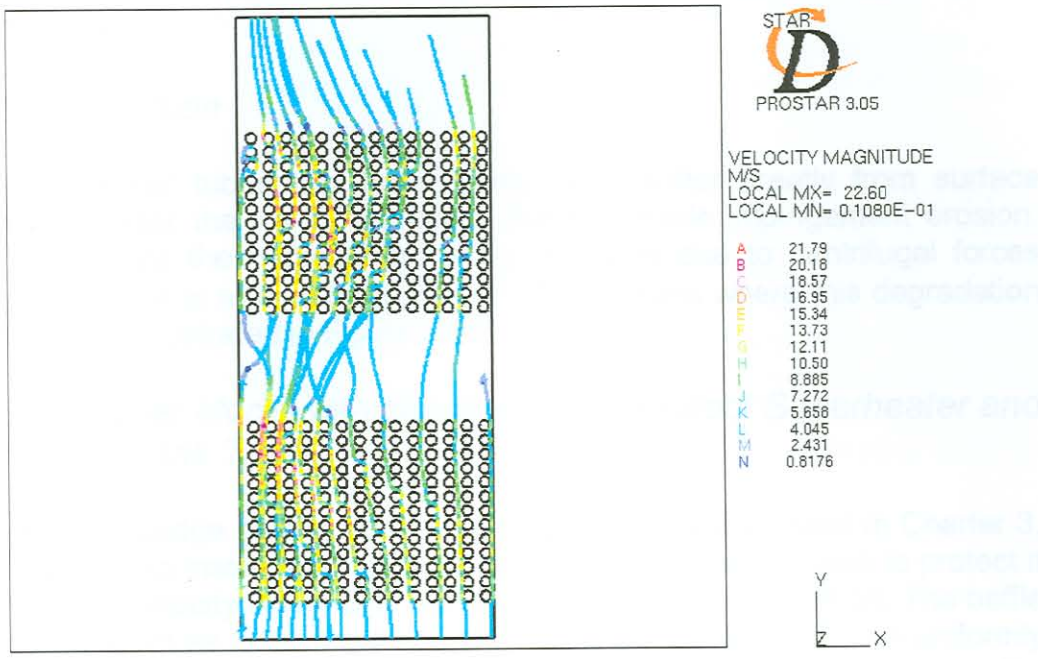

Figure 5-24 Particle Trajectories for 10μm Particles for 5m.s^{-1} Inlet Velocity

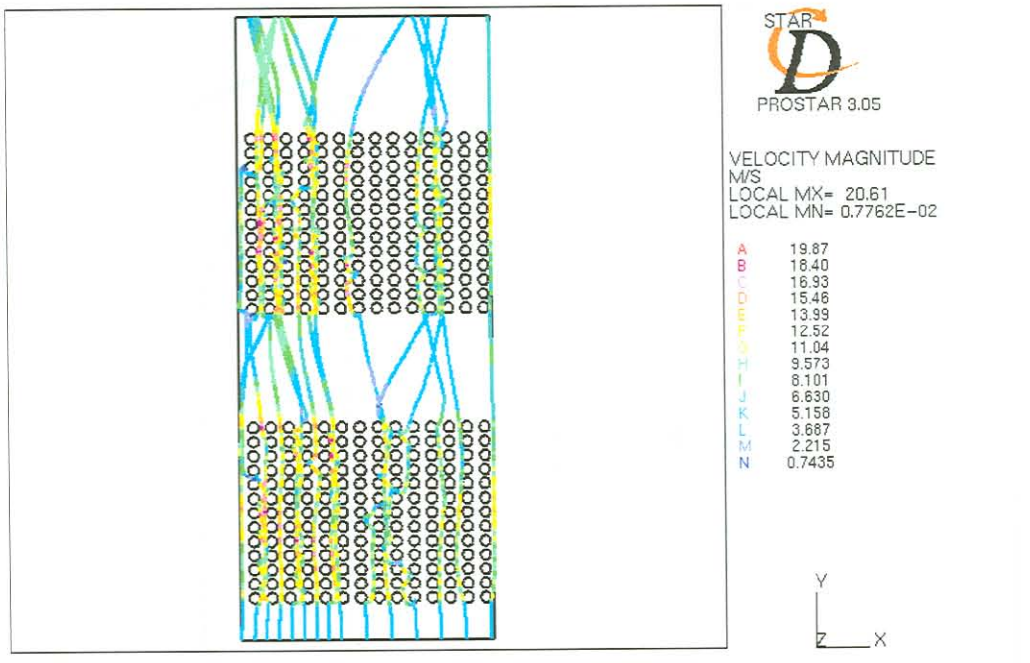

Figure 5-25 Particle Trajectories for 100μm Particles for 5m.s^{-1} Inlet Velocity

5.3 Remedial Measures for Superheater and Tube Bank Erosion

5.3.1 Introduction

The superheater tubes and boiler bank tubes suffer greatly from surface degradation near the top of the boiler due to particle impingement erosion. That is because the particles are flung outwards due to centrifugal forces because the flow is turning through 180°. The regions where this degradation take place are illustrated in Figure 5-26.

5.3.2 2D Boiler Model with Small Baffle to Protect Superheater and Tube Bank Tubes

From the knowledge gained from the literature survey discussed in Charter 3, it was decided to install a screen in front of the superheater tubes to protect it from the high velocity flow with a high fly-ash particle concentration. The baffle will hopefully act as a device that will redistribute the fly-ash more uniformly across the superheater and boiler bank tubes. Figure 5-26 illustrates the position of the baffle used for the protection of boiler tubes.

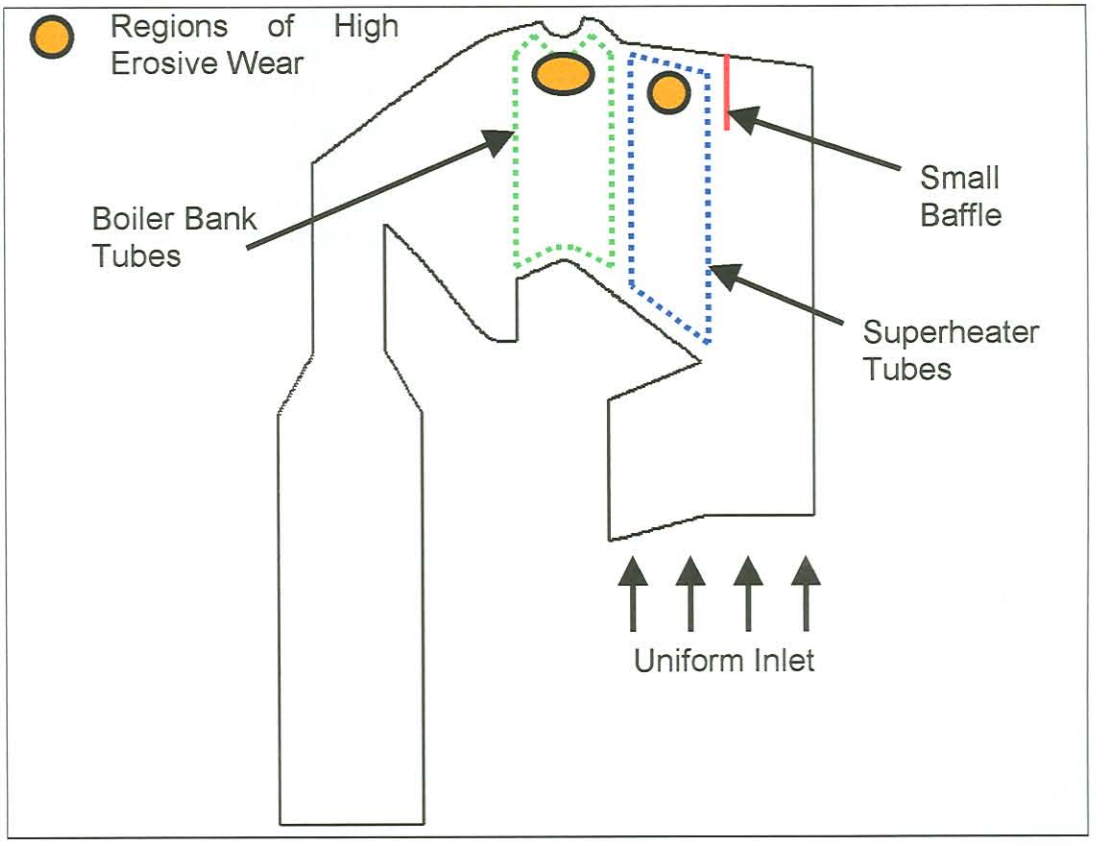

Figure 5-26 Schematic Diagram showing the Position of Tubes ,Small Baffle and Regions of High Erosive Wear in the Upper Boiler

5.3.2.1 Solid Baffle

Dooley and Westwood[**29**] warned that the use of solid baffles can cause movement of erosion to an adjacent area. Nevertheless, it is a useful first analysis to see if the baffle has the desired effect on the flow pattern through the boiler.

Figure 5-27 illustrates the velocity magnitude field for a 2D model of the boiler without any flow-modification devices. A large recirculation zone is evident above the bullnose. The region where high superheater tube wastage occurs is indicated with the circle in Figure 5-27. Figure 5-28 shows the plot of velocity magnitude with the installed solid baffle. The recirculation above the bullnose is much smaller but there is now essentially no flow in the top of the boiler leading to a loss in heat transfer to the wall tubes. There is also a large region of high velocity as indicated by the circle. This can possibly lead to tube wastage by erosion in those regions.

The particle traces for 100μm and 10μm particles for the boiler geometry with the solid baffle can be seen in Figure 5-29 and Figure 5-30 respectively. It is clear that the particle trajectories are essentially the same in the upper boiler for the different size particles. There are no particles in the recirculation zone above the bullnose or near the top of the boiler. It is now possible that erosion might be prevalent in this region because the particle and velocity distributions are not uniform across the superheater and boilerbank tubes but are concentrated in the middle section. A solid baffle is therefore not appropriate for the prevention of erosion. It can next be investigated what the flow patterns would be if the baffle were permeable or of a different size. The size of the baffle was arbitrarily chosen. Mathematical optimisation can be used to design the baffle to have the optimum size and permeability to obtain a uniform flow across the tube bank.

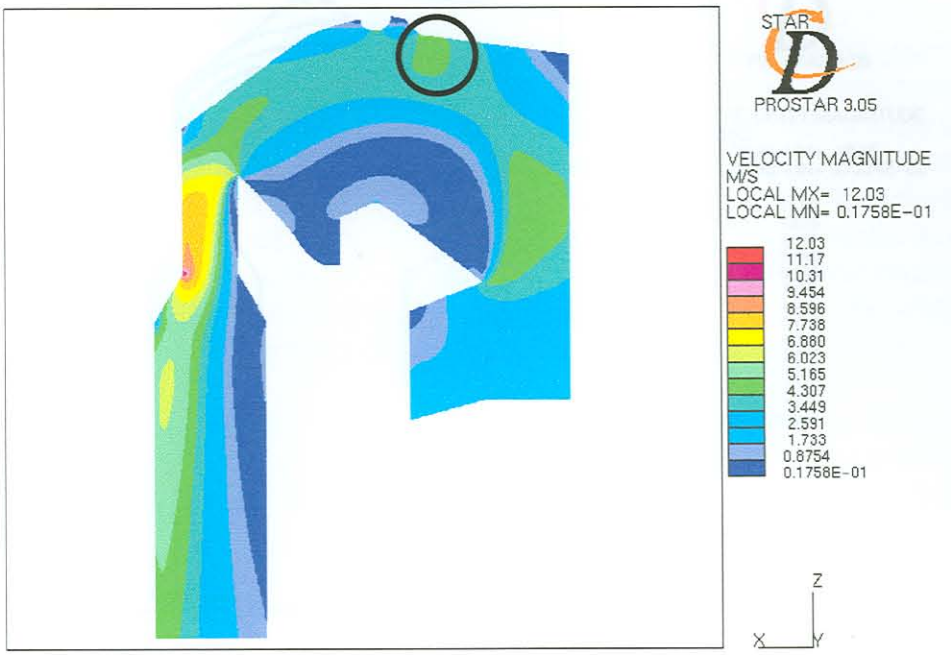

Figure 5-27 Velocity Magnitude Contour Plot without any Flow-Modification Devices ($2m.s^{-1}$ Inlet Velocity)

Figure 5-28 Velocity Magnitude Contour Plot with Solid Baffle ($2m.s^{-1}$ Inlet Velocity)

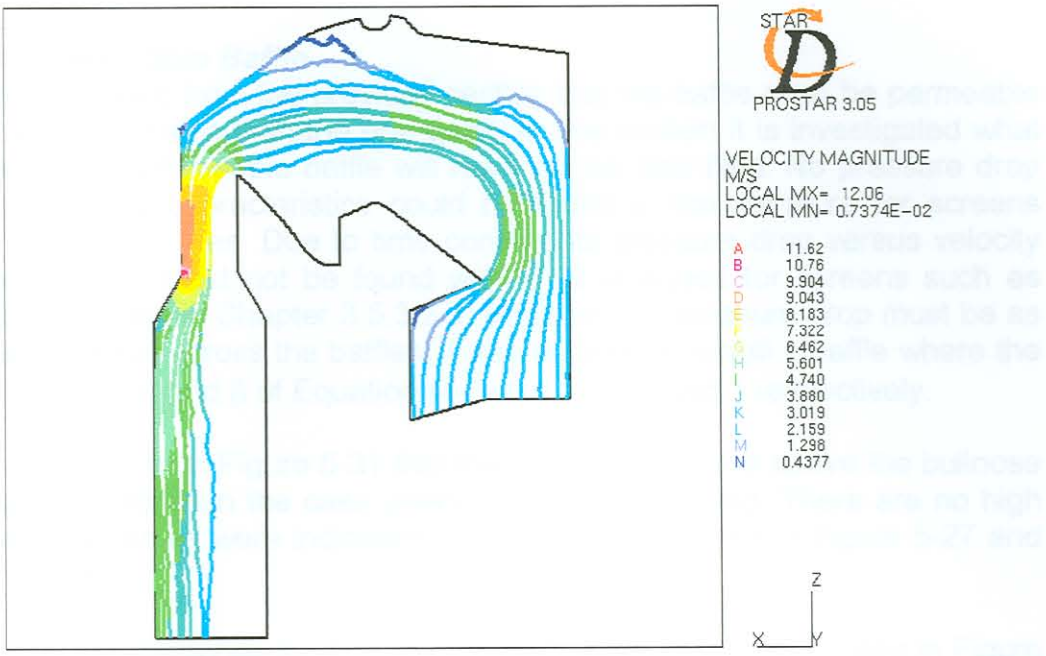

Figure 5-29 Particle Trajectories of 100μm Particles with Solid Baffle (2m.s^{-1} Inlet Velocity)

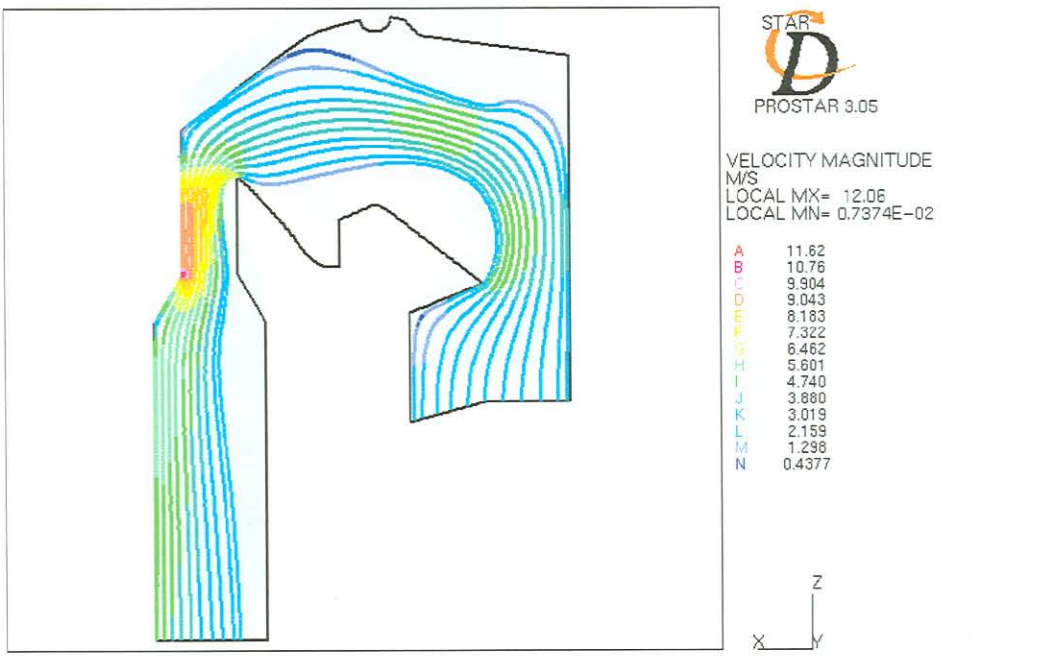

Figure 5-30 Particle Trajectories of 10μm Particles with Solid Baffle (2m.s^{-1} Inlet Velocity)

5.3.2.2 Permeable Baffle

It was concluded from the previous section that the baffle must be permeable or of a different size than the one used. In this section it is investigated what effect a small permeable baffle will have on the flow field. No pressure drop versus velocity characteristics could be found in the literature for screens used in boiler utilities. Due to time constraints pressure drop versus velocity characteristics could not be found with CFD analyses for screens such as those mentioned in Chapter 3.5.3.2.5. Because the pressure drop must be as little as possible across the baffles, it was decided to install a baffle where the coefficients of α and β of Equation (4-5) are 1.5555 and 1 respectively.

It can be seen from Figure 5-31 that the recirculation zone above the bullnose is much smaller than the case where no baffle was used. There are no high velocities areas as were indicated in the circles illustrated in Figure 5-27 and Figure 5-28.

The particle trajectories for 100μm and 10μm particles are illustrated in Figure 5-32 and Figure 5-33 respectively. The different sizes particles follow almost the same trajectories in the upper boiler, with the 100μm particles flung outwards just a bit more than the 10μm particles. If these results are compared to Figure 4-14 and Figure 4-15, the case where no baffles were used, it can be seen that the flow is more uniform across the tube bank.

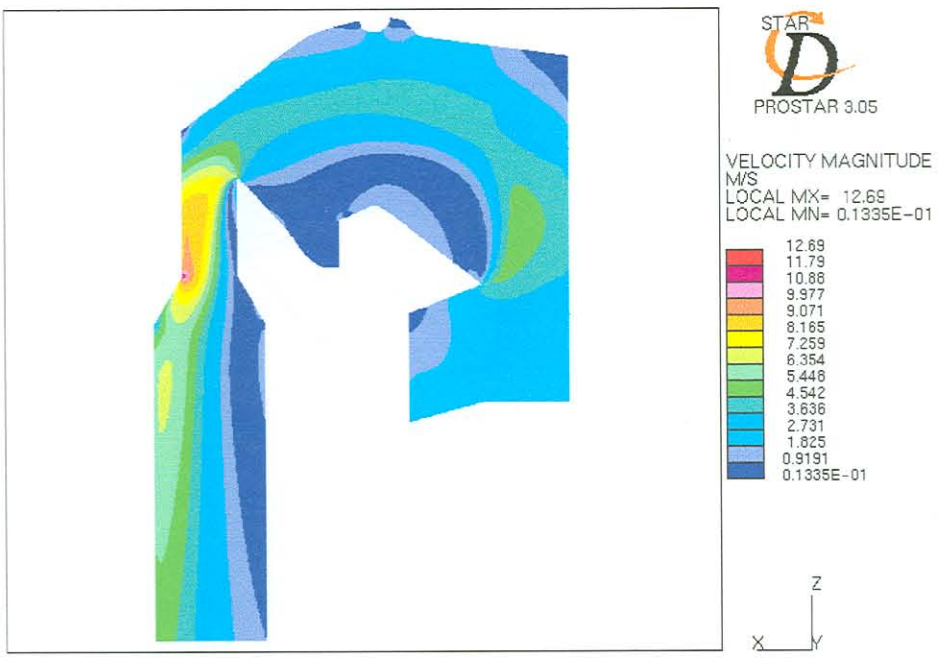

Figure 5-31 Velocity Magnitude Contour Plot with Permeable Baffle (2m.s^{-1} Inlet Velocity)

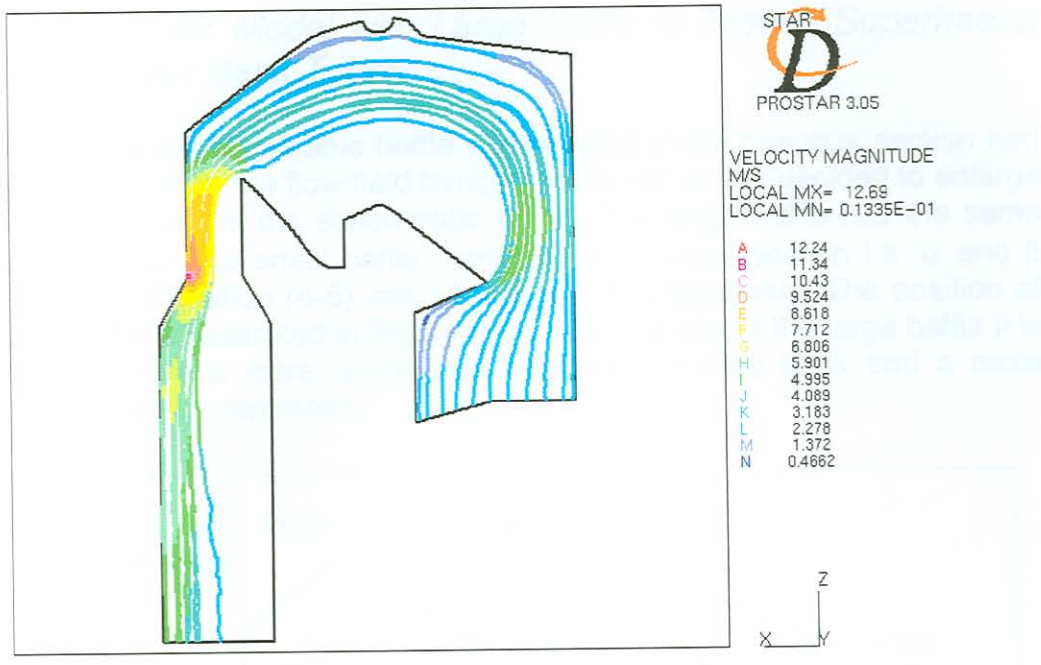

Figure 5-32 Particle Trajectories for 100μm Particles for Boiler Model with Permeable Baffle

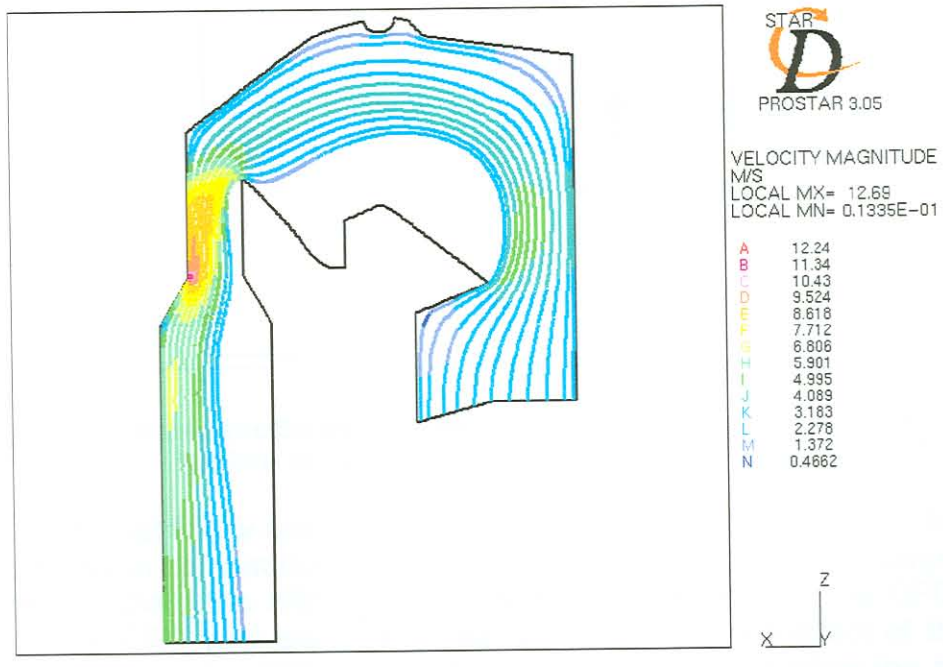

Figure 5-33 Particle Trajectories for 10μm Particles for Boiler Model with Permeable Baffle

5.3.3 2D Boiler Model with Large Baffle to Protect Superheater and Boiler Bank Tubes

Although the small permeable baffle investigated in the previous section had the desired effect on the flow field through the boiler, it was decided to enlarge the baffle to cover all the superheater tubes. The large baffle has the same permeability than the small baffle used in the previous section i.e. α and β coefficients of Equation (4-5) are 1.5555 and 1 respectively. The position of the large baffle is illustrated in Figure 5-34. With the use of the large baffle it is hoped to achieve a more uniform flow across the tube bank and a more uniform particle concentration.

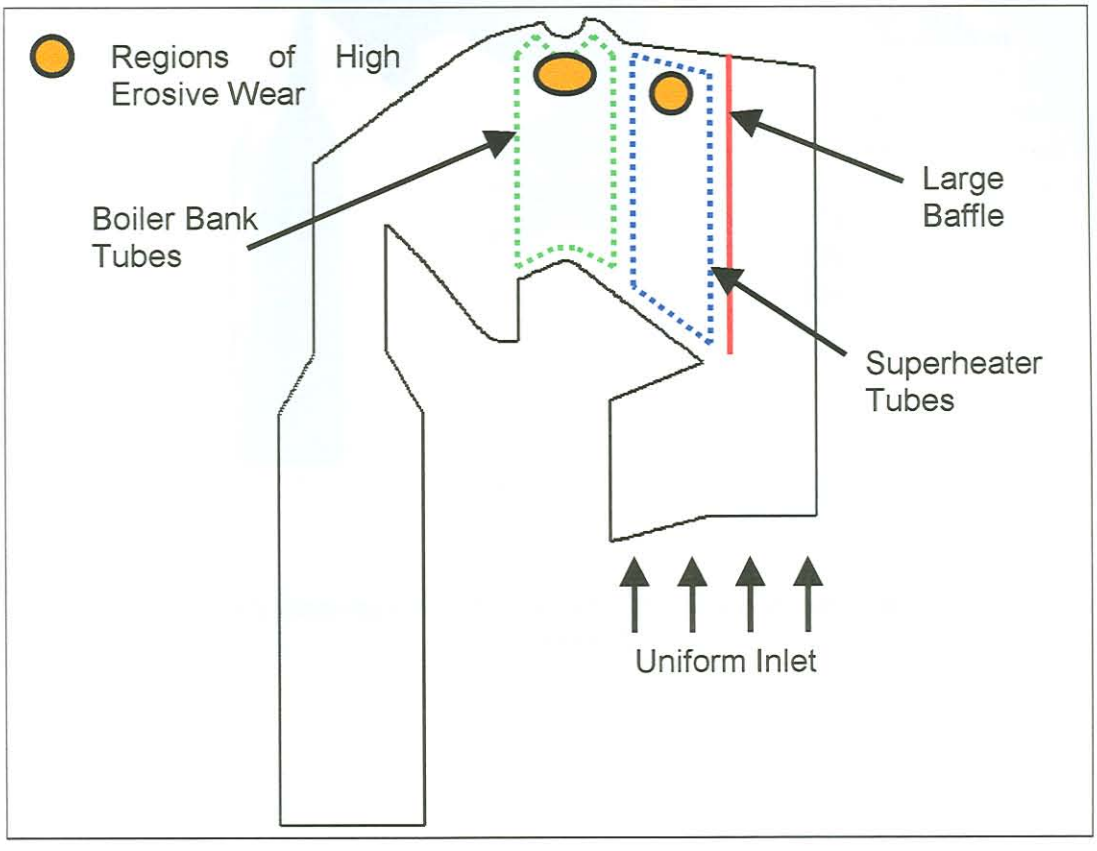

Figure 5-34 Schematic Diagram showing the Position of Tubes ,Large Baffle and Regions of High Erosive Wear in the Upper Boiler

The results that follow are the results where a large baffle is used in the CFD boiler model to combat boiler tube erosion. The results are also compared to the results where the effect of the tube bank is included in the CFD boiler model. The CFD analysis is then repeated with only the effect of the tube bank included in the CFD model. This is done to see whether the baffle is effective. Although it was concluded in Chapter 4 that the usage of porous cells, to model the effect of the tube bank, was not reliable at this stage, it was decided to see what effect the tube bank has on boiler flows. This is done because the screens as well as the tube bank are a resistance to flow in the tube bank, and both cause a pressure to drop across these devices.

Figure 5-35 shows the velocity magnitude contour plot where the large baffle is included in the CFD boiler model. If this velocity field is compared to Figure 5-31, the case where the small permeable baffle was used, it can be seen that there is not a large difference in the size of the recirculation zone above the bullnose. The recirculation zone for the case with the large permeable baffle is only a bit smaller than the case with the small permeable baffle.

Figure 5-35 Velocity Magnitude Contour Plot for Boiler Model with Large Baffle (2m.s^{-1} Inlet Velocity)

The following three figures show the particle traces for 100μm particles through the boiler for three different cases. Figure 5-36 illustrates the particle trajectories for the case where a large permeable baffle is included in the CFD model. Figure 5-37 illustrates the case where the large baffle is used, but this time the effect of the tube bank is included in the model through a porous section. To test the effectiveness of the baffle, Figure 5-38 illustrates the particle traces through the boiler with the effect of the tube bank included in the CFD model but with no baffle.

If the particle traces of Figure 5-36 are compared to Figure 5-32, it can be seen that the particles are similarly distributed across the tube bank. The small permeable baffle is far more effective than the large baffle because it has almost the same effect on particle trajectories but is much smaller and thus more cost effective to implement.

Figure 5-37 illustrates the particle traces where the effect of the tube bank is included in the CFD model together with the large baffle. It can be seen that the particles are distributed more uniformly across the tube bank than the CFD model where there is no tube bank in the model. To test the effectiveness of the large baffle, it was removed from the CFD model. Only the effect of the tube bank is included in the CFD model. The particle trajectories are shown in Figure 5-38 for this case. The particles are flung outwards towards the top of the boiler more than was the case where the large baffle was included in the model. It can thus be concluded that this baffle will distribute 100μm particles more uniformly across the tube bank whether the effect of the tube bank is included in the CFD model or not.

Figure 5-36 Particle Trajectories of 100μm Particles for Boiler Models with Large Baffle

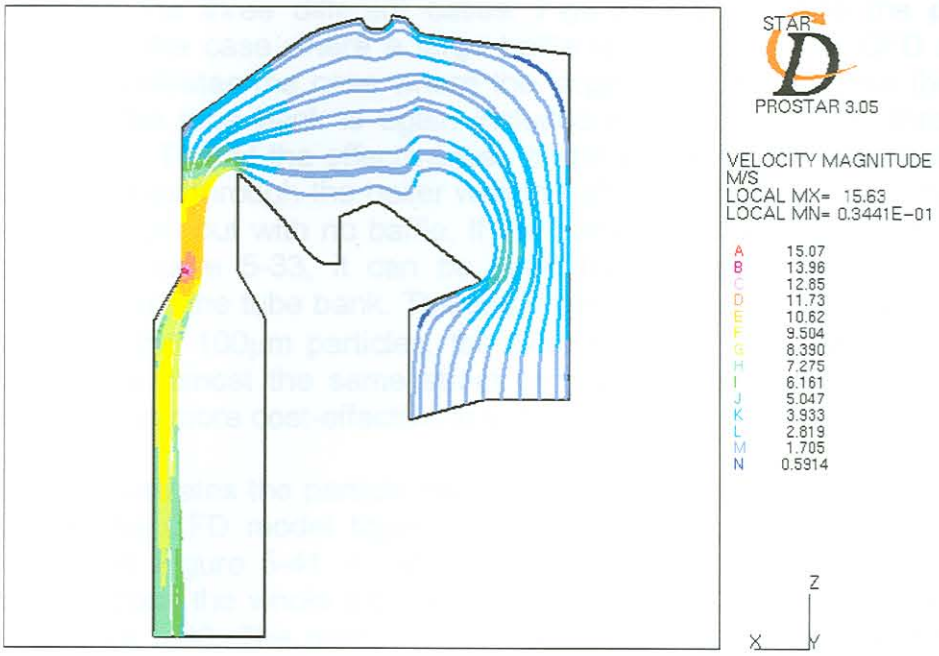

Figure 5-37 Particle Trajectories for 100μm Particles for Boiler Model with Large Particles – Effect of Boiler Bank Included in Model

Figure 5-38 Particle Trajectories of 100μm Particles with only the Effect of the Boiler Bank Included in the CFD Boiler Model

The following three figures show the particle traces for 10μm particles through the boiler for the three different cases. Figure 5-39 contains the particle trajectories for the case where a large baffle is included in the CFD model. Figure 5-40 illustrates the case where the large baffle is used, but this time the effect of the tube bank is again included in the CFD model through a porous section. To test the effectiveness of the baffle, Figure 5-41 illustrates the particle traces through the boiler with the effect of the tube bank included in the CFD model but with no baffle. If the particle traces of Figure 5-39 are compared to Figure 5-33, it can be seen that the particles are similarly distributed across the tube bank. The small permeable baffle is again, as was the case with the 100μm particles, far more effective than the large baffle, because it has almost the same effect on particle trajectories but is much smaller and thus more cost-effective to implement.

Figure 5-40 illustrates the particle traces where the effect of the tube bank is included in the CFD model together with the large baffle. If this result is compared with Figure 5-41, it can be seen that the particles are uniformly distributed across the whole tube bank in the crossflow direction as was the case in Figure 5-40. The major difference is in the size of the recirculation zone. When no large baffle is used, the recirculation zone is larger than the recirculation zone when a baffle is used. This will have an effect on superheater tube erosion because the superheater is just above the bullnose. It can thus be concluded that the large baffle will distribute 10μm particles more uniformly across the superheater tubes. The results are effective to obtain a uniform distribution across the superheater and tube bank whether the effect of the tube bank is either included or omitted in the CFD model.

Figure 5-39 Particle Trajectories of 10μm Particles for Boiler Model with Large Baffle

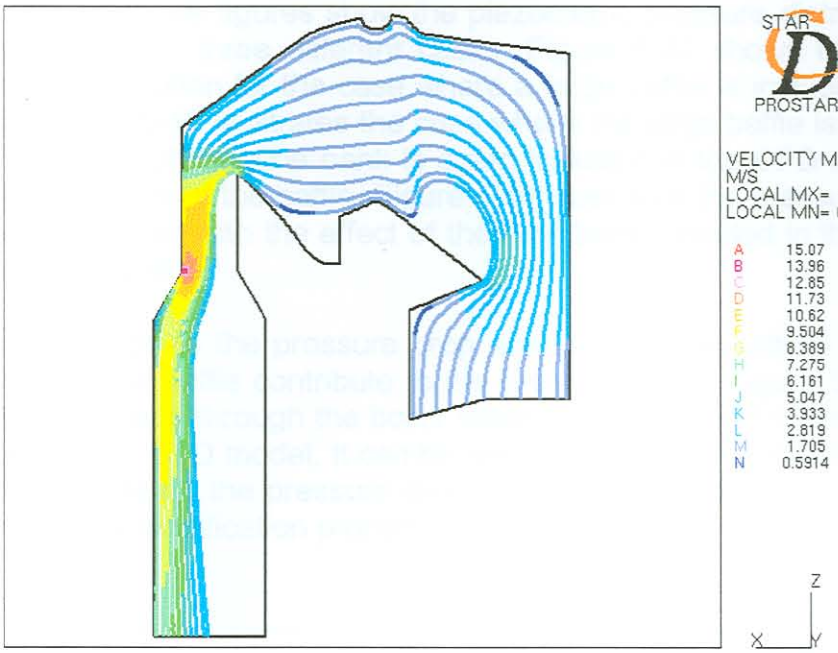

Figure 5-40 Particle Trajectories for 10μm Particles for Boiler Model with Large Particles – Effect of Boiler Bank Included in Model

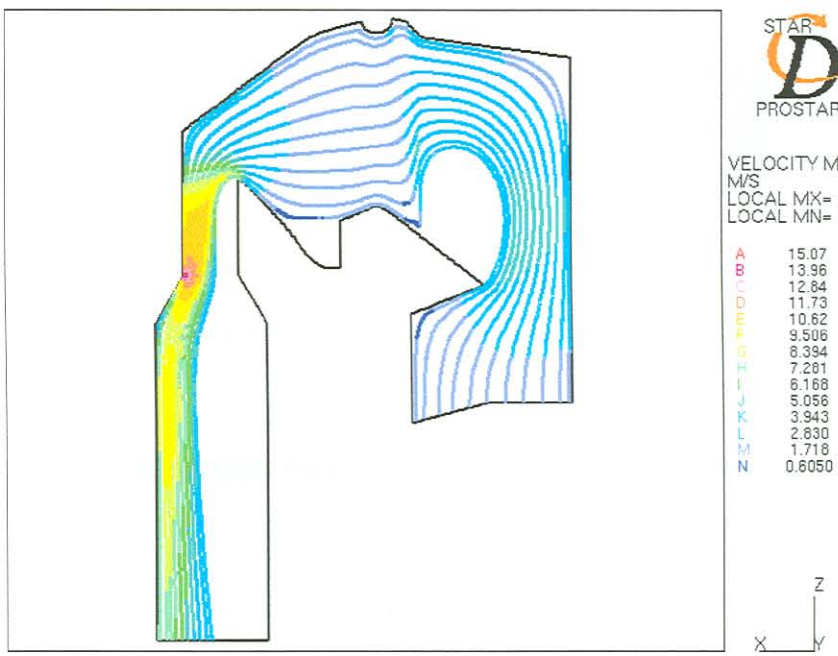

Figure 5-41 Particle Trajectories of 10μm Particles with only the Effect of the Boiler Bank Included in the CFD Boiler Model

The following three figures show the piezometric pressure distribution across the boiler for the three different cases. Figure 5-42 shows the piezometric pressure distribution for the case where a large baffle is included in the CFD model. Figure 5-43 illustrates the case where the large baffle is used, but this time the effect of the tube bank is again included in the CFD model. To test the effectiveness of the baffle, Figure 5-44 illustrates the pressure distribution through the boiler with the effect of the tube bank included in the CFD model but with no baffle.

Figure 5-43 shows the pressure drop across the boiler where both the tube bank and large baffle contribute to the pressure drop. Figure 5-44 illustrates the pressure drop through the boiler where only the effect of the tube bank is included in the CFD model. It can be seen from these results that the effect of the large baffle on the pressure drop is almost negligible even though it has desirable flow modification properties.

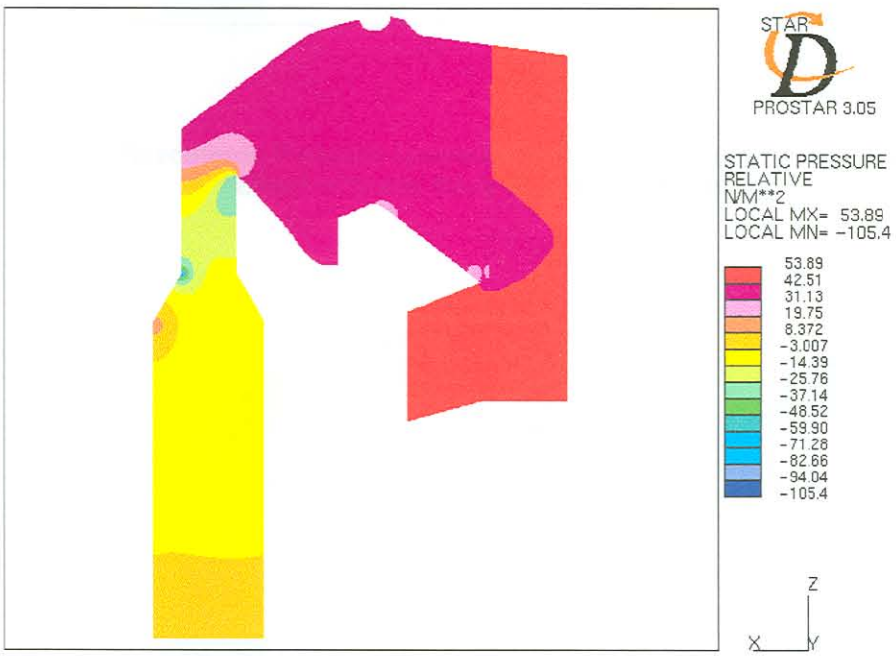

Figure 5-42 Piezometric Pressure Conrour Plot for Boiler Model with Large Baffle

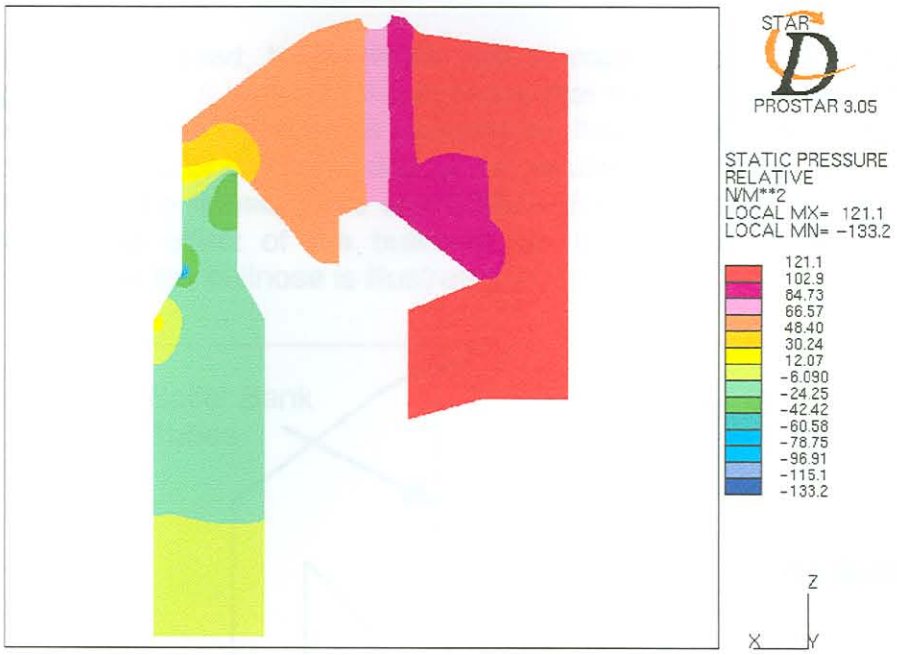

Figure 5-43 Piezometric Pressure Conrour Plot for Boiler Model with Large Baffle-Effect of Boiler Bank Included in Model

Figure 5-44 Piezometric Pressure Contour Plot with only the Effect of the Boiler Bank Included in the CFD Boiler Model

5.3.4 Removal of the Bullnose

As already discussed, the bullnose has a major effect on the flow pattern through the boiler. It is due to the bullnose that there is channelled flow in the top section of the boiler. This channelled flow is the main contributor to erosion in the top of the boiler due to the resulting high velocities and particle concentration. To remedy tube degradation due to erosion, it was decided to investigate the effect of the bullnose by removing it. The computational domain without the bullnose is illustrated in Figure 5-45.

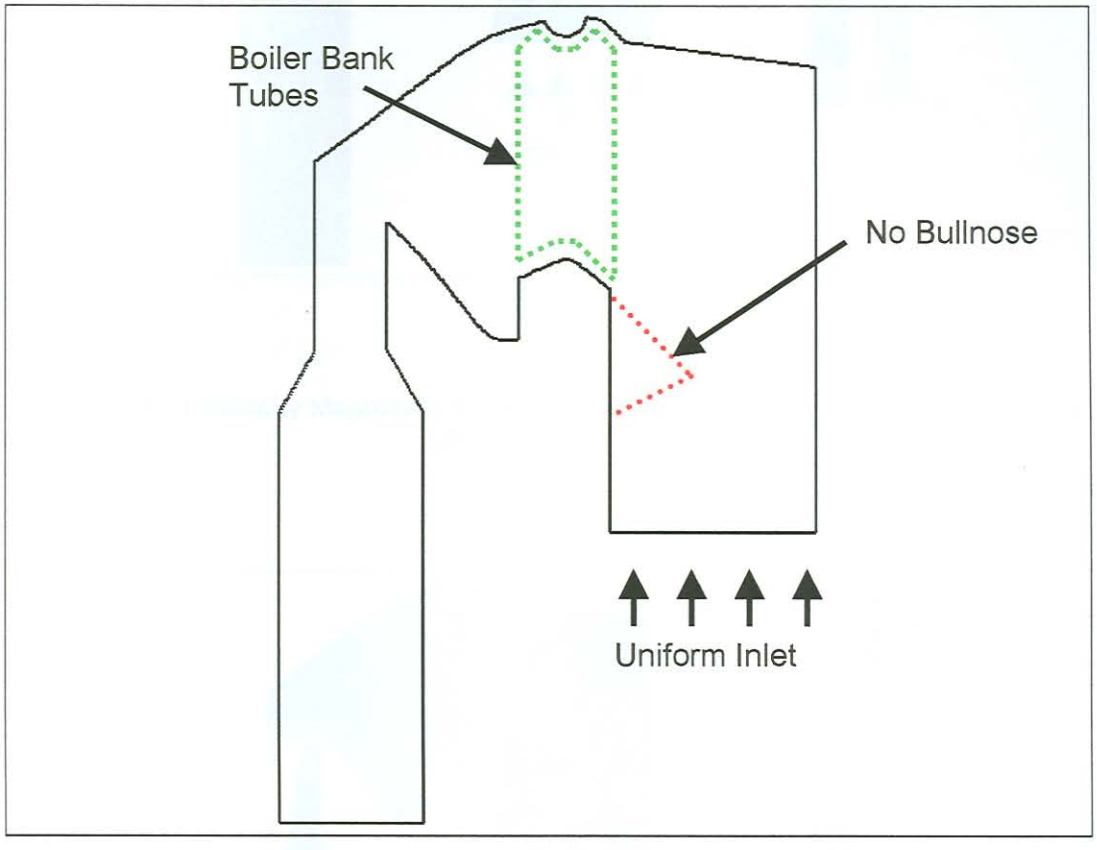

Figure 5-45 Computational Domain for Boiler Geometry without Bullnose

From the velocity magnitude plot in Figure 5-46, it can be seen that there exists no channelled flow in the top of the boiler. There is, however, a large dead volume section in the top right-hand corner of the boiler that was much smaller when the bullnose was included in the boiler CFD model.

Figure 5-47 shows the velocity magnitude contour plot where the effect of the tube bank is included in the CFD model. Although there are some concerns about the reliability of the porosity of the tube bank in the CFD model, as discussed in Chapter 4, it gives an indication of the effect of the tube bank on boiler flows. It can be seen that the dead volume section in the top right-hand corner of the boiler is almost the same as was the case in Figure 5-46 where the effect of the tube bank was not included in the model. The flow across the tube bank is much more uniform than the case where no tube bank was modelled.

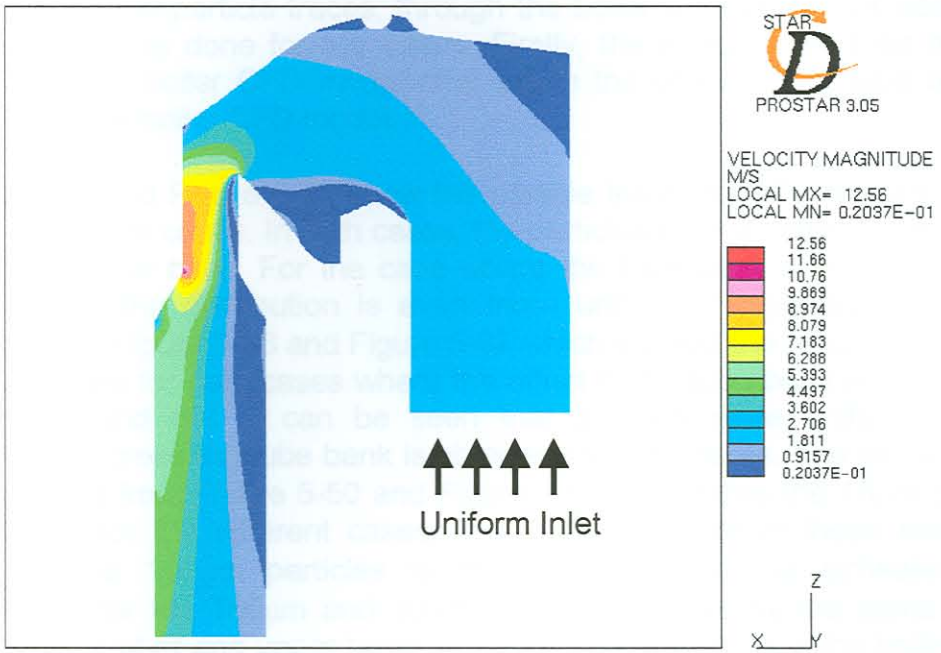

Figure 5-46 Velocity Magnitude Contour Plot of Boiler Geometry without Bullnose ($2m.s^{-1}$ Inlet Velocity)

Figure 5-47 Velocity Magnitude Contour Plot of Boiler Geometry without Bullnose. The Effect of the Boiler Bank Included in CFD Boiler Model ($2m.s^{-1}$ Inlet Velocity).

Again, when the particle traces, through the boiler without the bull nose, are investigated, it is done for two cases. Firstly, the effect of the tube bank is omitted in the boiler CFD model after which the effect of the tube bank is included in the boiler CFD model.

Figure 5-48 and Figure 5-49 show the particle traces for 100μm particles for the two different cases. In both cases, the particles have a uniform distribution across the tube bank. For the case where the tube bank is included in the CFD model, the distribution is even more uniform. These results can be compared to Figure 5-36 and Figure 5-37 which showed the results for 100μm particle traces for both cases where the effect of the tube bank is included in the model and not. It can be seen that a much more uniform particle distribution across the tube bank is obtained for both cases. The same trends are obtained from Figure 5-50 and Figure 5-51 that shows the 10μm particle trajectories for the different cases. The only difference in these results to those of the 100μm particles is the trajectories in the airheater. The trajectories for the 100μm and 10μm particles are exactly the same in the radiation chamber and upper boiler when there is a bullnose in the boiler.

With the removal of the bullnose in the boiler, channelled flow in the top of the boiler is eliminated. The distribution of all size particles is uniform across the tube bank. Erosion will be minimised considerably if the bullnose could be removed from the boiler because there are no regions of high velocity and high particle concentration in the upper boiler. The removal of the bullnose will have great cost implications but could prove viable in the long run. As screens can be used to minimise localised boiler tube erosion, at the fraction of the cost, the removal of the bullnose it is recommended as a remedial measure only if the other remedial measures fail to combat tube erosion effectively. The main reason for the existence of the bullnose, as mentioned in Chapter 3, namely the shielding of the tube bank and superheater from furnace radiation, should also be kept in mind when suggesting such major re-designs.

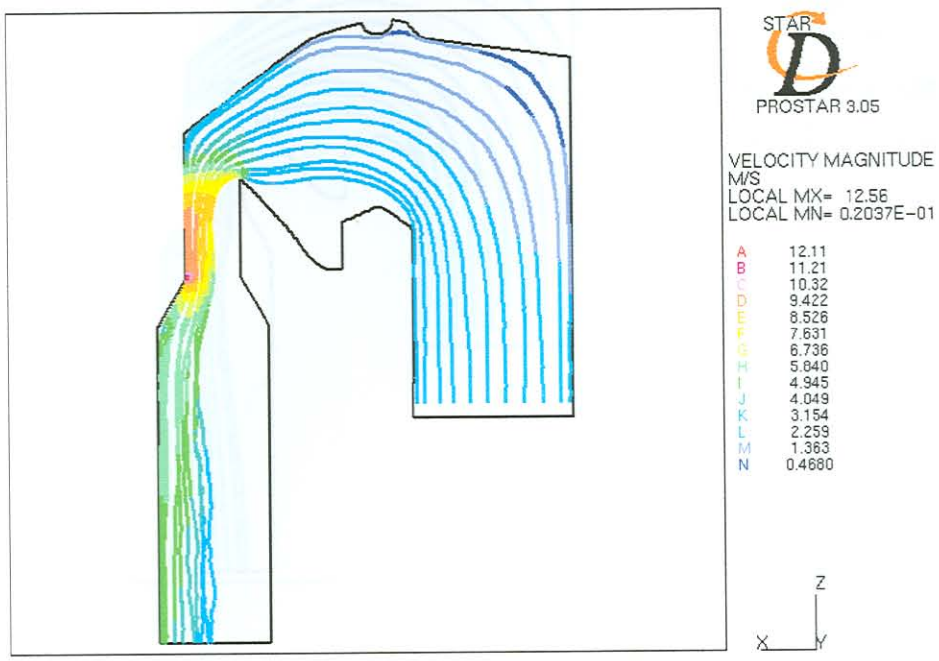

Figure 5-48 Particle Trajectories of 100μm Particles for Boiler Geometry without Bullnose

Figure 5-49 Particle Trajectories of 100μm Particles for Boiler Geometry without Bullnose. The Effect of the Boiler Bank Included in CFD Boiler Model.

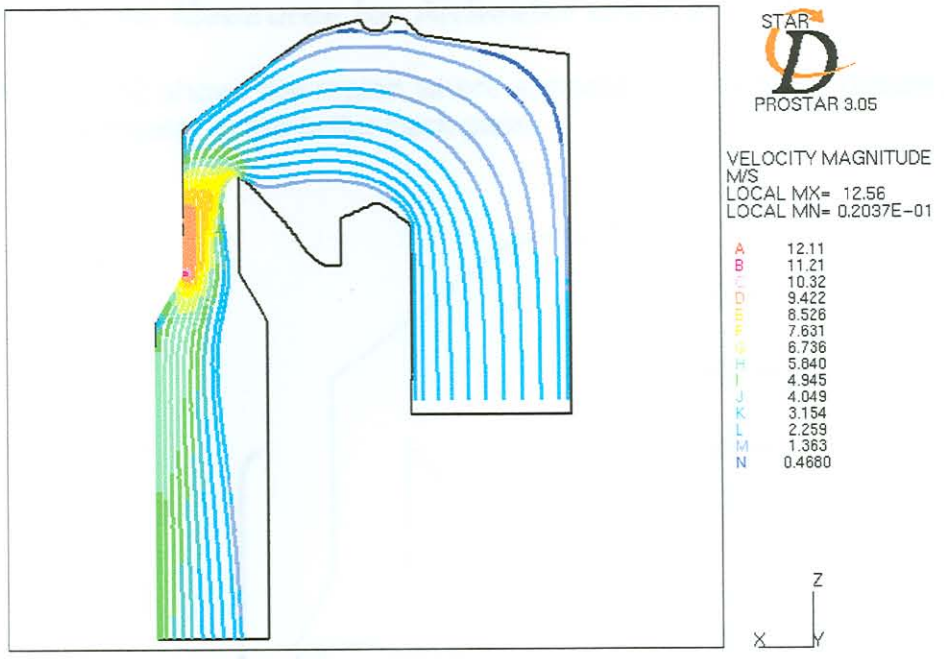

Figure 5-50 Particle Trajectories of 10μm Particles for Boiler Geometry without Bulnose

Figure 5-51 Particle Trajectories of 10μm Particles for Boiler Geometry without Bulnose. The Effect of the Boiler Bank Included in CFD Boiler Model

5.4 Remedial Measures for Airheater Erosion

The Figure 5-52 shows the region where airheater tube erosion occurs at the inlet of the airheater in the boiler back pass.

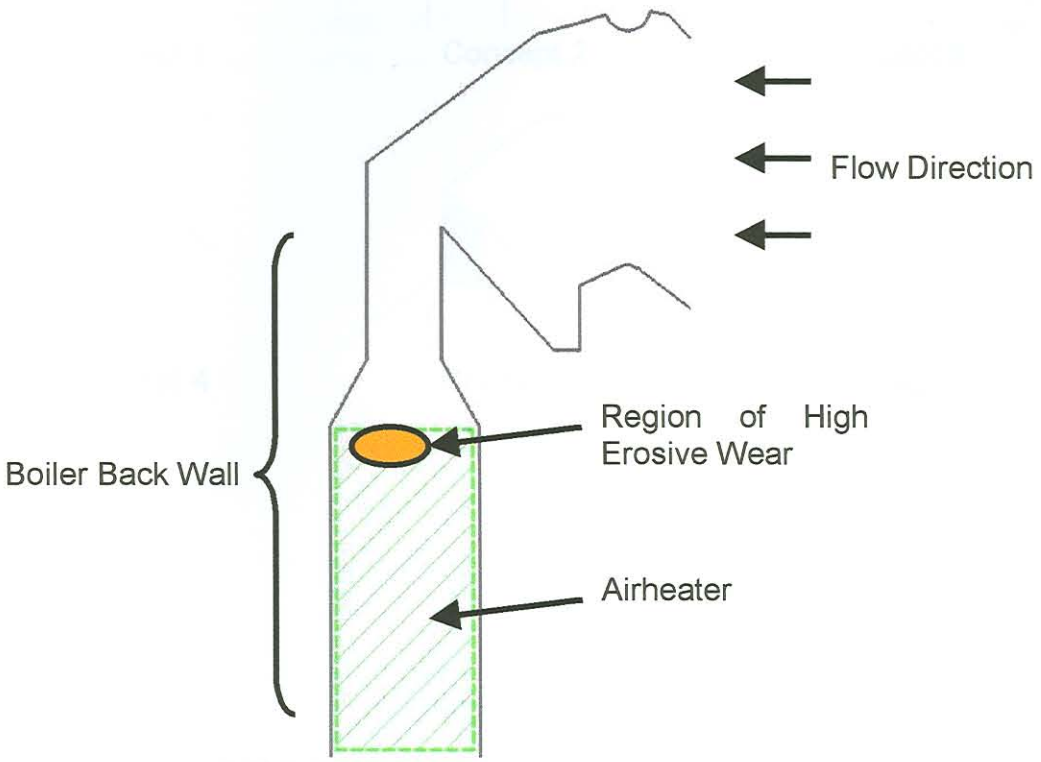

Figure 5-52 Diagram showing Regions of High Erosive Wear in the Airheater

Again it is believed that a skewed velocity field distribution and high particle concentration are the main contributors to erosion in the boiler back pass. The particles are flung against the boiler back wall due to centrifugal forces. The location of the boiler back wall can be seen in Figure 5-52. The rest of this section describes two concepts to successfully alleviate airheater tube erosion. Seven different concepts were investigated to reduce tube degradation due to particle erosion in the boiler back pass of which the two best concepts are discussed in the main text while the other less successful concepts are discussed in detail in Appendix C. All these concepts involve flow-modification approaches. Figure 5-53 illustrates the different flow modifying concepts of which Concepts 6 and 7 are the most successful ones to reduce airheater tube erosion. The effect of the tube bank is not modelled in this comparative investigation because the flow in the boiler back pass shows very similar tendencies due to the flow turning. This can be seen by comparing the particle trajectories in Figure 4-12 and Figure 4-13 for 10μm and 100μm particles respectively where no tube bank was modelled, to Figure 4-45 and Figure 4-46 respectively, where the effect of the tube bank is included in the CFD model.

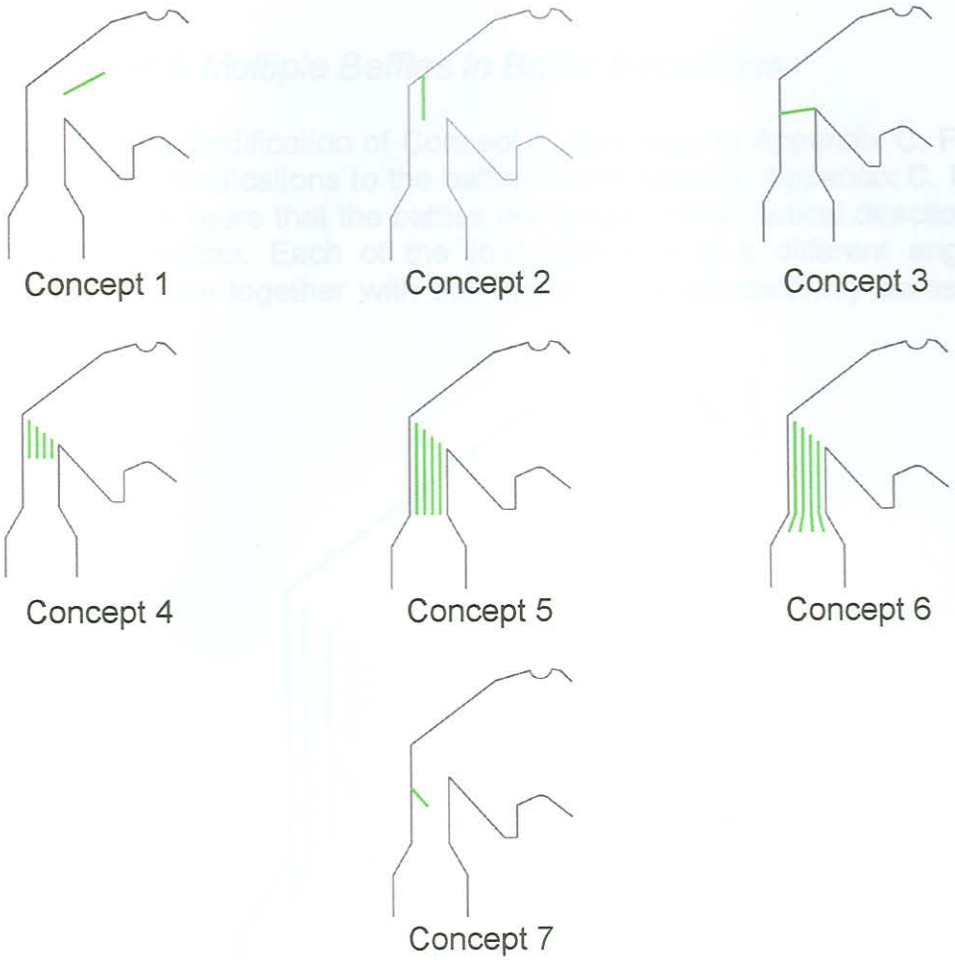

Figure 5-53 Different Concepts to Alleviate Airheater Erosion

The boiler can still be operational after an airheater tube failure because there is gas on both sides of the airheater tubes. The pressure difference between the gas phases is not so high that it can lead to other problems within the boiler. It is thus not critical if these tubes fail contrary to the case where there is water or steam under high pressure in the tubes, such as the superheater and tube bank tubes. If these tubes fail the boiler must be shut down. It is, nevertheless, still important to find remedial measures for these tube failures as continuous tube degradation can lead to major failures across the entire airheater in the long run which can severely affect boiler operational integrity.

5.4.1 Concept 6:Multiple Baffles in Boiler Back Pass

This concept is a modification of Concept 5 discussed in Appendix C. Figure 5-54 shows the modifications to the baffles investigated in Appendix C. It can be seen from this figure that the baffles are longer in the vertical direction but angled at the bottom. Each of the four baffles is at a different angle to redistribute the flow together with the fly-ash particles uniformly across the airheater.

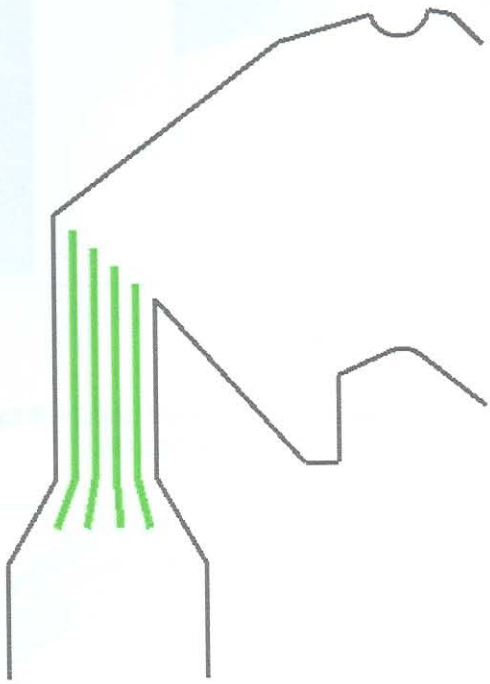

Figure 5-54 Concept 6: Location of Multiple Baffles in Boiler Back Pass – Modification to Concept 5

The velocity magnitude contour plot can be seen in Figure 5-55 for this concept. The maximum velocity in the flow domain increased by 3% from the results obtained in Concept 5 in Appendix C, but the particles are distributed more uniform across the airheater. Refer to Figure 5-56 and Figure 5-57 for the particle trajectories for this flow-modifying concept for 100μm and 10μm particles respectively.

Figure 5-55 Concept 6 – Long Vertical Baffles Angled at the Bottom: Velocity Magnitude Contour Plot

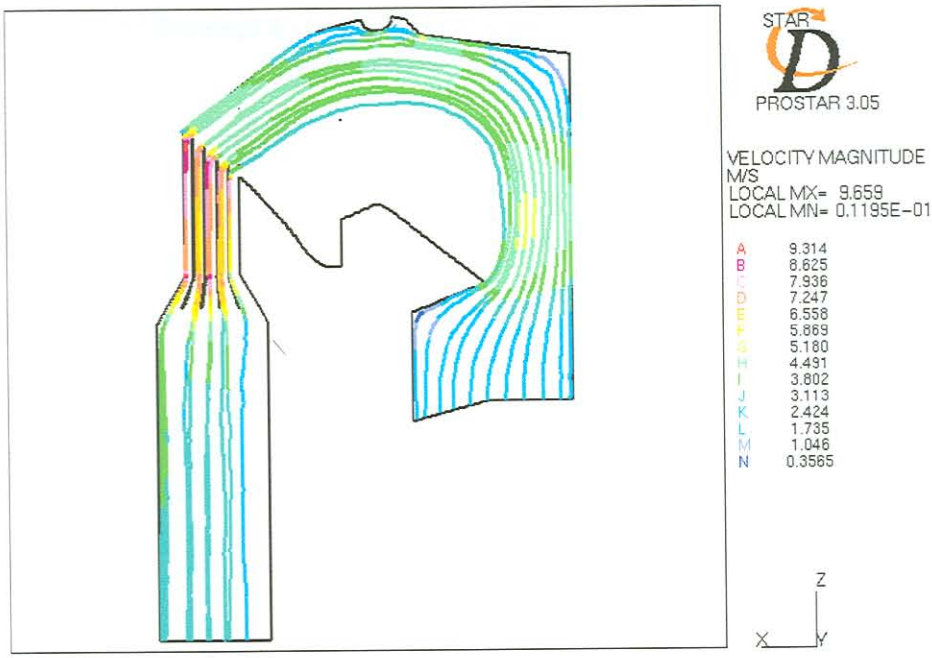

Figure 5-56 Concept 6 - Long Vertical Baffles Angled at the Bottom: Particle Trajectories of 100μm Particles

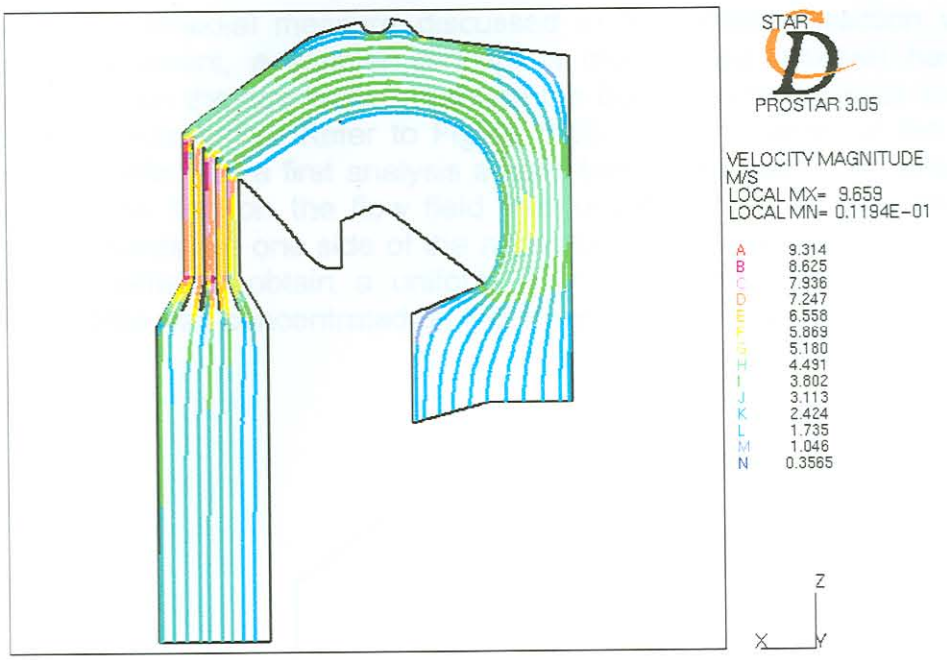

Figure 5-57 Concept 6 - Long Vertical Baffles Angled at the Bottom: Particle Trajectories of 10μm Particles

5.4.2 Concept 7: Permeable Baffle to Deflect the Flow

Because the remedial measure discussed in the previous section will be costly to implement, a simpler concept is investigated that will have the desired effect on the flow pattern through the boiler. It was decided to use a single permeable baffle. Refer to Figure 5-58 for the location of the single permeable baffle. For a first analysis a solid baffle was used. The effect that the solid baffle had on the flow field was unsatisfactory. All the flow was deflected towards the one side of the airheater. It was then decided to use a permeable baffle to obtain a uniform flow distribution, because the flow without a baffle was concentrated on the other side of the airheater.

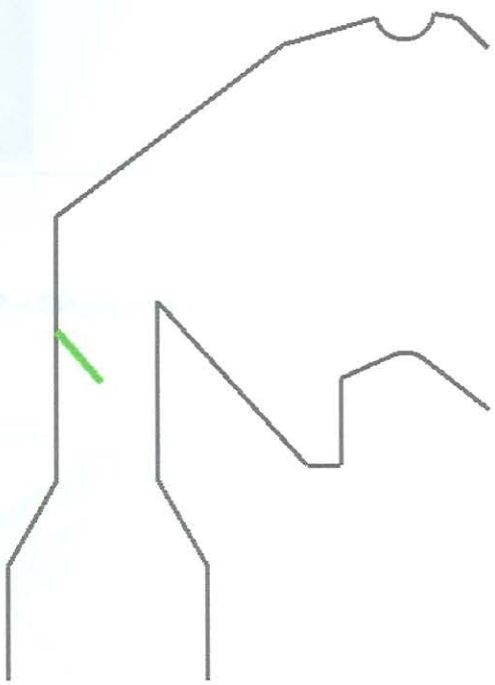

Figure 5-58 Concept 7: Solid Baffle to Deflect the Flow

It can be seen from Figure 5-59 that the maximum velocity in the flow domain is 8.127m.s^{-1}, which is a 32% decrease from the case where no flow-modifying approaches are used, which is illustrated in Figure 5-27. The region of high peak velocity is above the baffle but is dissipated before the flow interacts with the airheater tubes.

Figure 5-60 and Figure 5-61 illustrates the particle trajectories for 100μm and 10μm particles respectively. It is evident that the particles are distributed approximately uniformly across the airheater, especially in the 10μm case.

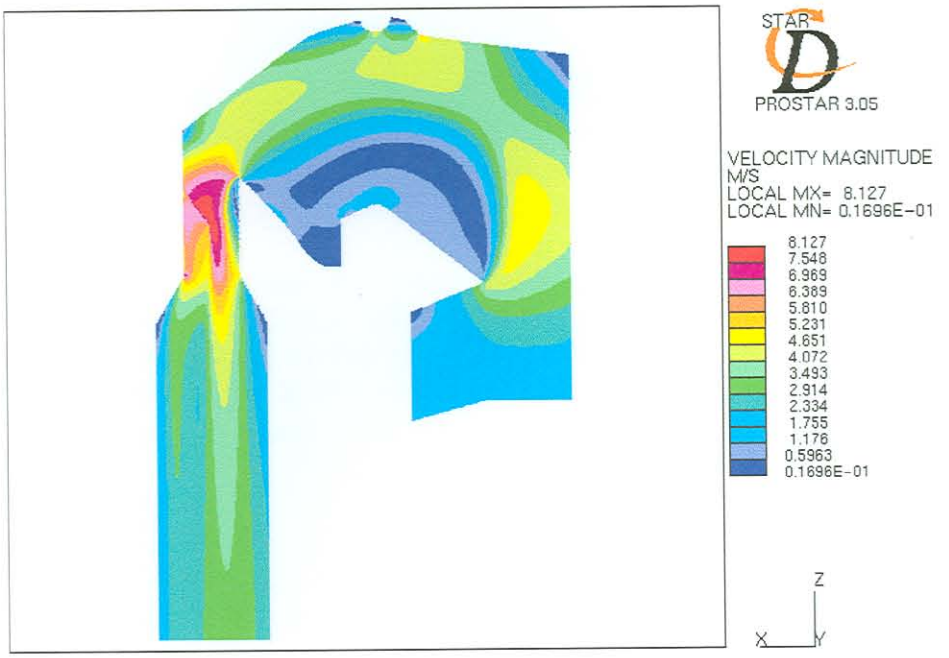

Figure 5-59 Concept 7 – Single Permeable Baffle: Velocity Magnitude Contour Plot

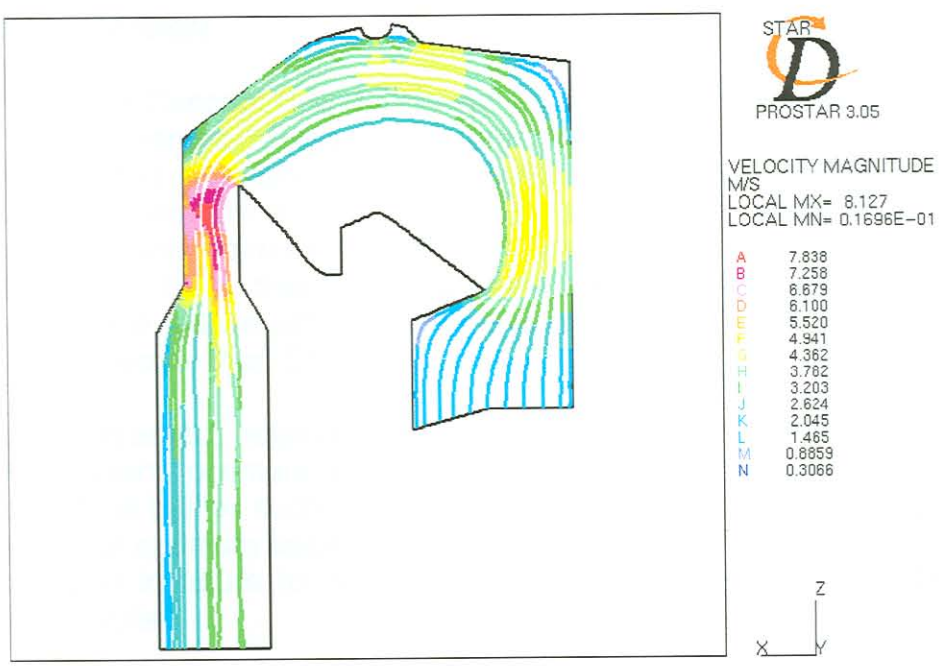

Figure 5-60 Concept 7 – Single Permeable Baffle: Particle Trajectories of 100μm Particles

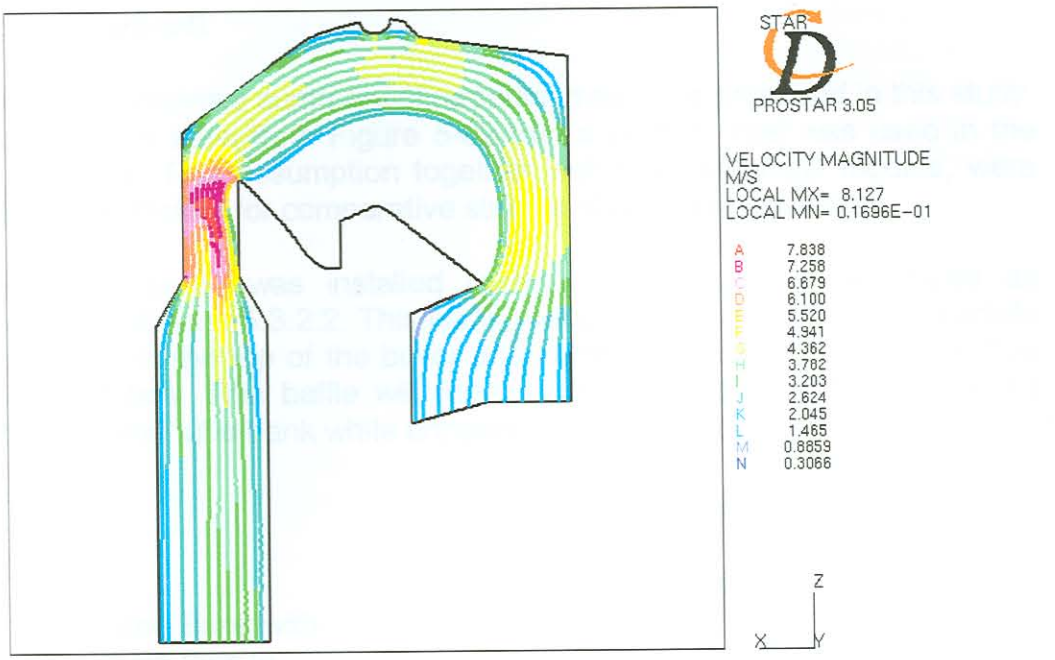

Figure 5-61 Concept 7 – Single Permeable Baffle: Particle Trajectories of 10μm Particles

5.4.3 Conclusion

The results of Concept 6 and Concept 7 investigated are both promising in obtaining permanent remedial measures for airheater tube erosion in the boiler back pass. Only one permeable baffle was used in Concept 7 whereas four large baffles with a more complex geometry were used in Concept 6. Both the concepts have essentially the same effect on the flow field through the airheater. It is therefore recommended that Concept 7 must be implemented to reduce airheater tube erosion because it is much simpler and more cost effective than Concept 6.

It must be stressed, however, that the concepts were arbitrarily chosen and do not present optimum solutions. As there are numerous parameters influencing the baffles such as permeability, size and location, it will be difficult to obtain real optimum solutions by trial-and-error. Mathematical optimisation can be used in future to optimise the baffle used in Concept 7 to obtain optimum results.

5.5 Conclusion

Figure 5-62 contains a summary of remedial measures proposed in this study. Firstly it can be seen from Figure 5-62 that a uniform inlet was used in the CFD analyses. This assumption together with the use of 2D models, were found to be sufficient for comparative studies of remedial measures.

A permeable baffle was installed in front of the superheater tubes as discussed in Chapter 5.3.2.2. This baffle reduces channelled flow and particle concentration in the top of the boiler and contributes to a more uniform flow across the tubes. This baffle will reduce particle erosion at the top of the superheater and tube bank while enhancing heat transfer across these tubes.

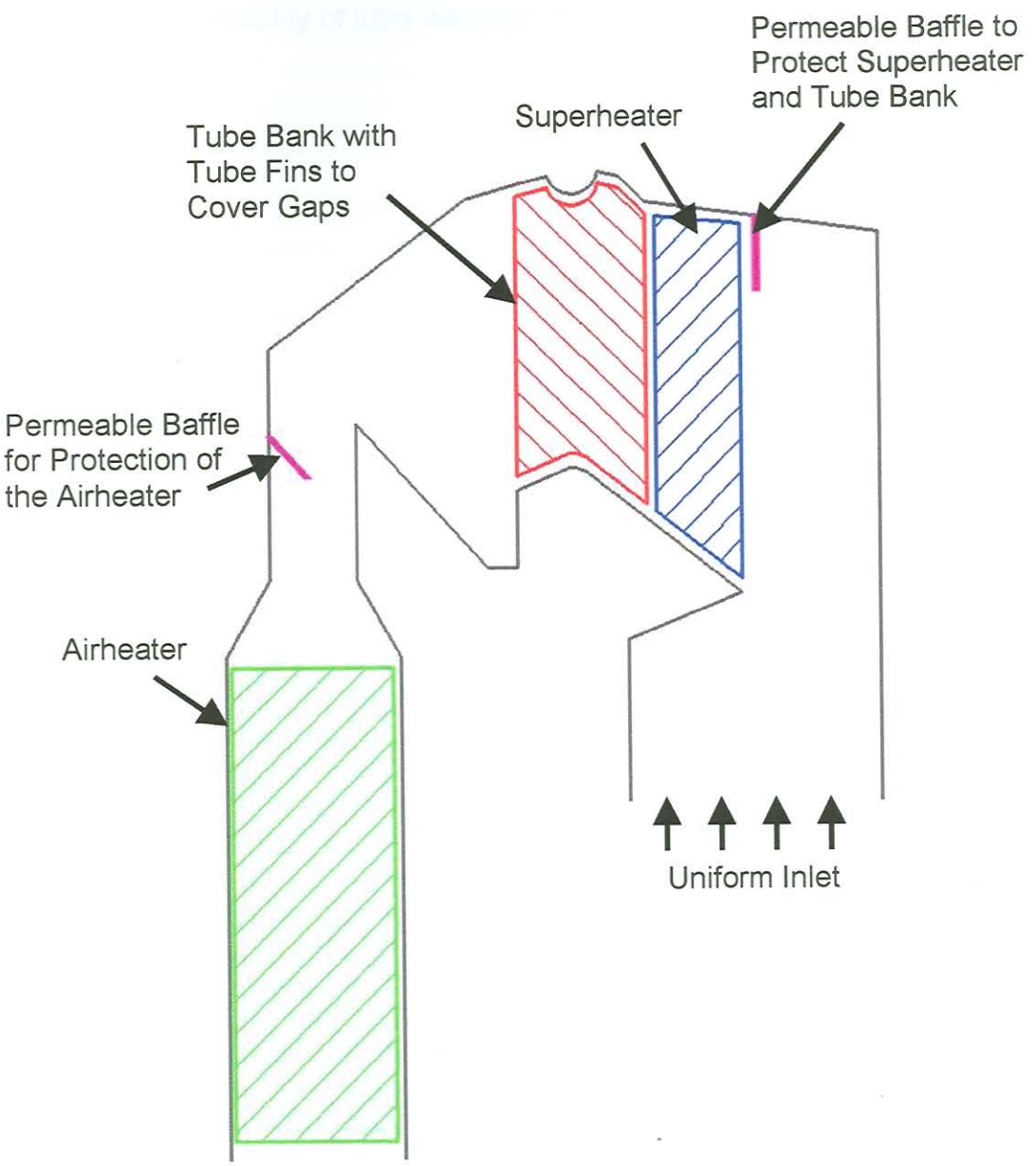

Figure 5-62 Summary of Remedial Measures for Boiler Tube Erosion

Because of the gaps in the tube bank the baffle could be ineffective to reduce erosion in those gaps. High erosion rates occur in regions adjacent to the larger than usual tube spacing because of channelling of the flow with a high particle concentration. As shown in Chaprter 5.2.4.2 tube fins must be installed, preferably on every second tube, to eliminate channelling of the flow that causes high peak velocities with high particle concentration of mainly small (in the region of 10μm) particles.

Airheater erosion, although not as critical as tube bank or superheater erosion, can be reduced by installing a permeable baffle, as indicated in the boiler back pass in Figure 5-62. This permeable baffle causes both the particle sizes considered to be more uniformly spaced across the airheater. If this baffle is not installed, the fly-ash concentration is high near the boiler back wall with a possibility of tube wastage in that region.